ADVANCED MATERIALS
www.advmat.de

Materials Views
www.MaterialsViews.com

REVIEW

Stretchable, Curvilinear Electronics Based on Inorganic Materials

By *Dae-Hyeong Kim, Jianliang Xiao, Jizhou Song, Yonggang Huang,** and *John A. Rogers**

All commercial forms of electronic/optoelectronic technologies use planar, rigid substrates. Device possibilities that exploit bio-inspired designs or require intimate integration with the human body demand curvilinear shapes and/or elastic responses to large strain deformations. This article reviews progress in research designed to accomplish these outcomes with established, high-performance inorganic electronic materials and modest modifications to conventional, planar processing techniques. We outline the most well-developed strategies and illustrate their use in demonstrator devices that exploit unique combinations of shape, mechanical properties and electronic performance. We conclude with an outlook on the challenges and opportunities for this emerging area of materials science and engineering.

1. Introduction

Progress in much of silicon electronics is dominated by a development path that involves doubling the number of transistors in microprocessors every 18–24 months[1] Continuing this trend, known as Moore's Law, requires solutions to many interesting challenges in materials science and engineering.[2] This class of electronics is important, but it is not the only one. In the early 1990s, large area, thin film silicon (i.e., amorphous silicon) electronics on glass emerged to serve as an active switching matrix for pixels in liquid crystal displays.[3] This sort of application is impossible to address with Moore's Law technology because the required area coverages greatly exceed those that are economically possible with silicon wafers. In this type of system, sometimes known as macroelectronics, the primary scaling metric is overall size (i.e., bigger is better for many display applications) rather than critical dimensions of individual transistors or their packing density. This technology began its growth nearly forty years after the birth of silicon microelectronics, yet it now captures a rapidly growing market that represents a sizable fraction of the entire, broader semiconductor industry.[4,5]

Many believe that an important future in electronics is with systems that avoid the rigid, brittle and planar nature of existing classes of both micro and macroelectronics, to enable new applications. Research in this direction began ~15 years ago,[6,7] originally motivated primarily by interest in flexible, paperlike displays.[8–13] More recently, the scope has expanded to include more compelling, and more technically challenging, opportunities such as those in biomedical devices that intimately integrate with the human body and in product designs that exploit curvilinear, ergonomic or bio-inspired layouts. One approach to such technology involves the development of new electronic materials, such as organic semiconductors or films of carbon nanotubes/graphene that can flex[11,14–19] and composite elastomer conductors that can stretch.[20,21] Work in these areas is reviewed in a companion article in the same journal.[22] Here, we summarize strategies that use optimized structural configurations of established, high-performance inorganic materials. The concepts that enable stretchy properties from these brittle materials are simple, although the detailed mechanics can be complex.[23–25] Achieving bendability is a first step to

[*] Prof. Y. Huang
Department of Civil and Environmental Engineering, Northwestern University
Evanston, Illinois 60208 (USA)
E-mail: y-huang@northwestern.edu
Prof. Y. Huang, J. Xiao
Department Mechanical Engineering, Northwestern University
Evanston, Illinois 60208 (USA)
Prof. J. A. Rogers, D.-H. Kim
Department of Materials Science and Engineering
Beckman Institute for Advanced Science and Technology, and Frederick Seitz Materials
Research Laboratory, University of Illinois at Urbana-Champaign
Urbana, Illinois 61801 (USA)
E-mail: jrogers@uiuc.edu
Prof. J. A. Rogers
Department of Chemistry, Mechanical Science and Engineering
Beckman Institute for Advanced Science and Technology, and Frederick Seitz Materials
Research Laboratory, University of Illinois at Urbana-Champaign
Urbana, Illinois 61801 (USA)
Prof. J. A. Rogers
Department of Electrical and Computer Engineering
Beckman Institute for Advanced Science and Technology, and Frederick Seitz Materials
Research Laboratory, University of Illinois at Urbana-Champaign
Urbana, Illinois 61801 (USA)
J. Song
Department of Mechanical and Aerospace Engineering, University of Miami
Coral Gables, FL 33146 (USA)

DOI: 10.1002/adma.200902927

 © 2010 WILEY-VCH Verlag GmbH & Co. KGaA, Weinheim

stretchability. Any material, in sufficiently thin form, is bendable, by virtue of bending strains that are directly proportional to thickness. For example, a sheet of single crystalline silicon with 100 nm thickness (i.e., a nanomembrane) on a 20 μm-thick plastic substrate experiences peak strains of only 0.1% on bending to a radius of curvature of 1 cm,[26] which is well below the fracture limits for silicon (~1%). This strain can be reduced further, often by orders of magnitude, with designs that exploit neutral mechanical plane concepts or strain isolation schemes. These and related mechanics ideas provide the basis for inorganic bendable (or flexible, as we use the term here) electronics. Reviews of recent work in this area can be found elsewhere.[26,27]

Stretchability is more general, and more challenging, characteristic than flexibility. Stretchable circuits have the capacity to absorb large levels of strain (>>1%) without fracture or significant degradation in their electronic properties; they are also flexible, due to this mechanics. A general strategy to achieve such response at a device level in materials that are intrinsically brittle is to combine bendable designs, such as those described above, with layouts that enable motion out of the plane of the circuit. The resulting behavior resembles the response of an accordion bellows to applied strain.[23,28] In advanced forms, these and related ideas provide routes to inorganic electronics with the electrical properties of comparably designed wafer-based devices but with the mechanical properties of a rubber band.[29,30] This article begins with an overview of the materials and mechanics aspects of the most successful approaches of this type, and the properties of devices and small scale circuits that can be achieved. Following sections describe some integrated, system-level demonstrators. The conclusion provides some thoughts on scientific and engineering opportunities in this field.

2. Inorganic Materials in Stretchable Configurations

2.1. Buckling Strategy

With brittle inorganics, the only path to stretchability involves specialized structural layouts and mechanical designs. One of the most intuitive approaches exploits out-of-plane motion in thin layers to accommodate strains applied in the plane. Hybrid systems that use structures of inorganics with this mechanics, bonded to or embedded in elastomeric substrates exhibit reversible responses to large strain deformations. Broad ranges of stretchability are possible, with significant strains only in the elastomer. Figure 1 illustrates two examples of this design, as applied to arrays of thin ribbons. In the first case (Fig. 1a), initially flat ribbons are bonded at all points on their bottom surfaces to an elastomeric substrate that is mechanically (or thermally) strained along the lengths of the ribbons. Releasing the prestrain induces compressive forces on the ribbons that lead to a non-linear buckling response. The resulting 'wavy' deformations have well-defined wavelengths and amplitudes that are linearly proportional to the ribbon thickness h_f, and depend on the material properties and the level of prestrain. For relatively small

Yonggang Huang obtained B.S. degree in mechanics from Peking University, China, in 1984, and S.M. and Ph.D. degrees in engineering science from Harvard University in 1987 and in 1990, respectively. He has taught at several universities in the States, and is now the Joseph Cummings Professor jointly in the Department of Mechanical Engineering and Department of Civil and Environmental Engineering, Northwestern University. Huang's research includes mechanics modeling of advanced materials, devices and processes.

John A. Rogers obtained B.A. and B.S. degrees in chemistry and in physics from the University of Texas, Austin, in 1989. From MIT, he received S.M. degrees in physics and in chemistry in 1992 and a Ph.D. in physical chemistry in 1995. From 1995 to 1997, Rogers was a Junior Fellow in the Harvard University Society of Fellows. During this time he also served as a Director for Active Impulse Systems, a company based on his Ph.D. research that he co-founded in 1995, which was acquired by a large company in 1998. He joined Bell Laboratories as a Member of Technical Staff in the Condensed Matter Physics Research Department in 1997, and served as Director of this department from 2000–2002. He currently holds the Flory-Founder Chair in Engineering at the University of Illinois at Urbana-Champaign, with appointments in the departments of Materials Science and Engineering, Electrical and Computer Engineering, Mechanical Science and Engineering and Chemistry. Rogers' research includes fundamental and applied aspects of nano and molecular scale fabrication, materials and patterning techniques for unusual format electronics and photonic systems.

Dae-Hyeong Kim enrolled at the Seoul National University in the Chemical Engineering Department and received a B.S. degree and an M.S. degree in Feb 2000 and Feb 2002, respectively. After his graduation, he worked for a company, KCTech, as a research engineer and developed and mass produced the Ceria slurry for the shallow trench isolation chemical mechanical planarization process in the semiconductor manufacturing process. After four and a half years' work experience, he went on to pursue a Ph.D under the guidance of Professor John Rogers with support from the Samsung Scholarship Foundation.

© 2010 WILEY-VCH Verlag GmbH & Co. KGaA, Weinheim
WILEY InterScience DISCOVER SOMETHING GREAT

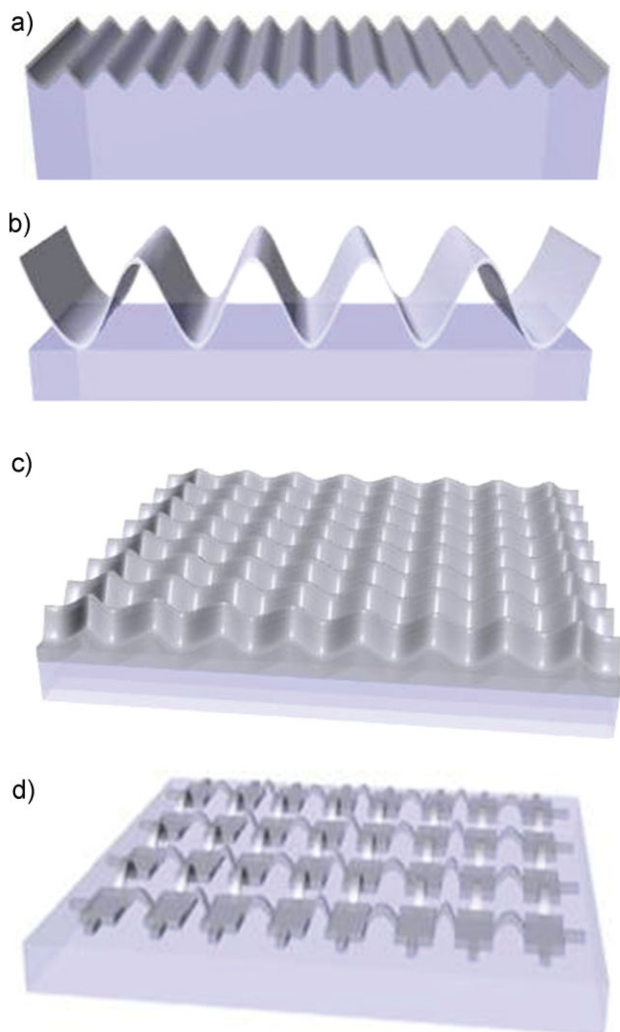

Figure 1. Schematic illustrations of different structural approaches to stretchable inorganic materials. a) One dimensional 'wavy' inorganic ribbon (grey) bonded to an elastomeric substrate (blue). b) One dimensional buckled inorganic ribbon bonded to an elastomeric substrate only at the positions of the troughs. c) Two dimensional 'wavy' membrane, as an extension of the concept illustrated in (a). d) Two dimensional buckled mesh, as an extension of the concept illustrated in (b). Here, only the rectangular islands are bonded to the elastomer.

prestrain ε_{pre} (<10%), the wavelength $\lambda_0 = 2\pi h_f\left[\overline{E}_f/(3\overline{E}_s)\right]^{1/3}$ depends only on the plane-strain moduli (the plane-strain modulus $\overline{E}$ is related to the Young's modulus E and Poisson's ratio ν by $\overline{E}_s = E_s/(1-\nu_s^2)$). $\overline{E}_f$ and $\overline{E}_s$ of the ribbon and substrate,[25] and the amplitude $A_0 = h_f\sqrt{\varepsilon_{pre}/\varepsilon_c - 1}$ increases with the prestrain ε_{pre}, where $\varepsilon_c = (3\overline{E}_s/\overline{E}_f)^{2/3}/4$ is the critical buckling strain, which is 0.036% for silicon ribbons on PDMS substrate. For large prestrain ε_{pre}, the wavelength decreases with ε_{pre} but the amplitude increases with ε_{pre}, and they are given by $\lambda = \lambda_0/\left[(1+\varepsilon_{pre})(1+\xi)^{1/3}\right]$ and $A = A_0/\left[\sqrt{1+\varepsilon_{pre}}(1+\xi)^{1/3}\right]$, where $\xi = 5\varepsilon_{pre}(1+\varepsilon_{pre})/32$.[23] In this configuration, the hybrid system can be stretched or compressed reversibly with a linear elastic response to strain. The amplitudes and wavelengths of the waves change to accommodate strains in a way that involves small or negligible strain in the ribbons, similar to an accordion. In a related strategy, the ribbons can be designed to bond to the elastomer only at certain locations (Fig. 1b). Here, releasing the prestrain leads to large, out-of-plane bridge structures, due to delamination of the non-bonded regions from the substrate. The wavelength λ is the same as the length of the non-bonded regions, $W_{non\text{-}bond}$.[28,31,32] The amplitude is obtained as $A \approx (2/\pi)\sqrt{W_{non-bond}[W_{non-bond} + W_{bond}(1+\varepsilon_{pre})]\varepsilon_{pre}/(1+\varepsilon_{pre})}$, where W_{bond} is the length of the bonded regions. The advantage of this layout is that the wavelengths can be defined precisely, in geometries that optimize the range of stretchability, with a level of engineering control that is absent from the case of Figure 1a. These two structure possibilities, as illustrated in Figure 1, appear quite different. In practical applications, however, they are similar, because both involve an elastomeric encapsulation layer applied on top, as described in Section 3.5.

Although the isolated ribbons of Figure 1a and 1b illustrate the basic mechanics aspects, they do not provide the foundation for an electronics technology because processing to form interconnects or other elements directly on an elastomeric substrate is prohibitively difficult. The same concepts, however, can be applied to two dimensional membranes or interconnected mesh structures, as shown in Figure 1c and d. Uniformly bonded sheets deform into wavy shapes with herringbone layouts, defined by two characteristic wavelengths, upon relaxation of biaxial strains in the substrate (Fig. 1c)[33] Mesh structures bonded at the locations of the islands adopt geometries that involve arc-shaped bridges as interconnects (Fig. 1d).[30] The detailed mechanics in these cases is more complex than that associated with the ribbons, but the intuition is the same: out-of-plane motion provides an ability to respond to strains applied in the plane. As shown in subsequent sections, these and more advanced structures can accommodate wide ranging modes of deformation with large strain ranges, without fracture.

Figure 2 illustrates experimental demonstrations of these concepts in ultrathin structures of single crystalline silicon and gallium arsenide. In both cases, the fabrication starts with the generation of these materials from high-quality bulk or layered wafers. As examples, silicon nanoribbons can be made with either silicon on insulator (SOI) wafers through undercut etching of the buried oxide,[26,34,35] or with bulk silicon wafers (111 direction) through anisotropic etching with KOH or TMAH.[36–38] Related processes can be used with other semiconductor materials, including GaAs,[39–43] InP,[40] GaN,[43,44] diamond,[45] carbon nanotubes,[46] carbon nanomembranes.[47] Transfer printing such materials to a prestrained substrate of the elastomer polydimethylesiloxane (PDMS) followed by release leads to the desired buckled structures, via patterned or unpatterned bonding.[26] The required adhesion can be achieved between layers of SiO_2 on the nanoribbons and hydroxylated surfaces of the PDMS.[31,48,49] Here, covalent −O−Si−O− chemical linkages form via condensation reactions between silanol (Si−OH) groups on the PDMS and similar groups on the SiO_2. The required funcationalization of PDMS is most readily accomplished using exposure to ozone, either uniformly or in selective, lithographically defined regions.[31]

Detailed theoretical analysis reveals all aspects of the mechanics of formation of such structures, as well as their responses to applied strains. A recent review article summarizes

© 2010 WILEY-VCH Verlag GmbH & Co. KGaA, Weinheim

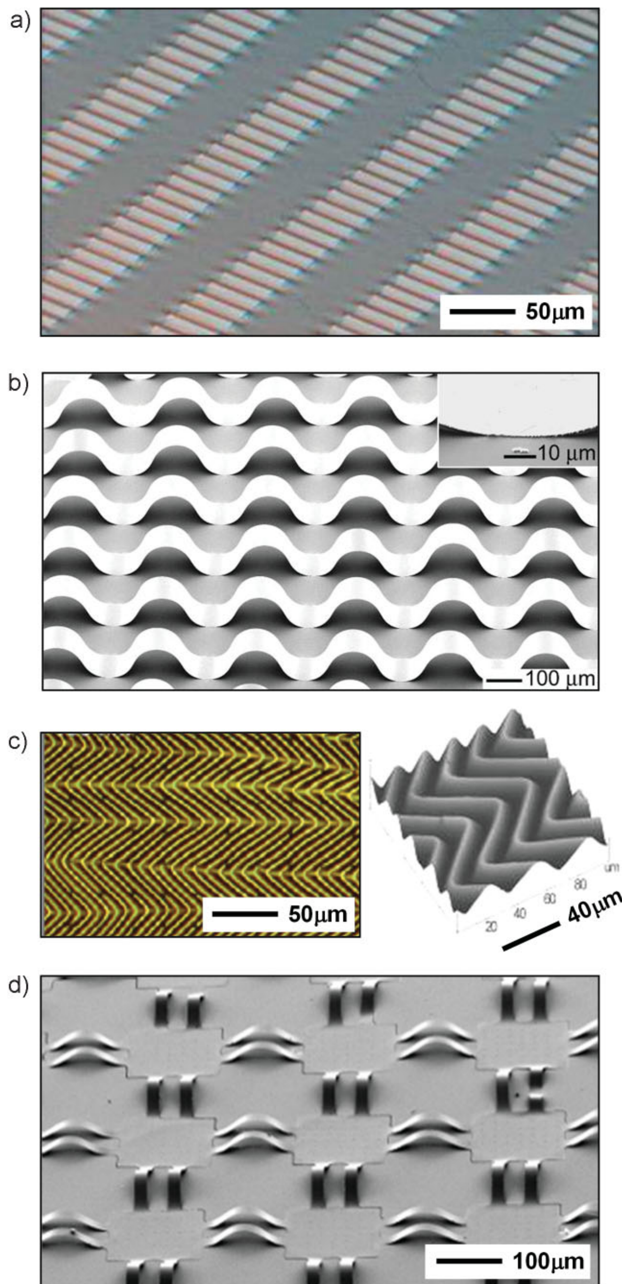

Figure 2. Scanning electron microscopy (SEM) and optical microscopy images of inorganic structures in controlled buckling geometries on elastomeric substrates. a) SEM image of an array of silicon nanoribbons in wavy configurations on PDMS. Reproduced with permission from ref. [28]. Copyright American Association for the Advancement of Science. b) SEM image of an array of gallium arsenide nanoribbons in buckled shapes where bonding to the PDMS substrate occurs only at the positions of the troughs, as illustrated in the top inset. Reproduced with permission from ref. [31]. Copyright Nature Publishing Group. c) Optical microscopy (left) and atomic force microscopy images (right) of a wavy, silicon nanomembrane bonded to a PDMS substrate. Reproduced with permission from ref. [33]. Copyright American Chemical Society. d) SEM image of a silicon nanomembrane in a buckled, mesh layout on PDMS. Bonding is localized to the regions of the square islands.

these results.[25] Briefly, for uniformly bonded systems, the maximum strain in the ribbon is $\varepsilon_{max} = 2\sqrt{\varepsilon_{pre}\varepsilon_c}$.[28] Since ε_c is typically very small (0.036% for silicon ribbons on PDMS substrate), the strain advantage associated with the wavy shapes provides a 10–20× improvement in the stretchablity for most inorganic semiconductors, compared to intrinsic values set by the fracture strains (~1%) of these materials. For example, wavy silicon structures can accommodate strain ranges of 15–20% before fracture. The selectively bonded systems can accommodate much larger strains. For the length of bonded regions much smaller than non-bonded regions (i.e., $W_{bond} << W_{non\text{-}bond}$), the maximum strain in the ribbon is $\varepsilon_{max} \approx 2\pi(1+\varepsilon_{pre})\sqrt{\varepsilon_{pre}}h_f/W_{non-bond}$.[28,31,32] In optimized designs ($h_f << W_{non\text{-}bond}$), strains of 100% or more, even to values approaching the fracture strain of the elastomer (i.e., PDMS), are possible.

2.2. Other Strategies

Stretchable inorganic structures that do not use, or are not specifically designed to exploit, out-of-plane motion are also possible.[50–52] One such approach utilizes coiled-springs, as demonstrated recently in silicon structures formed from the top silicon layer of an SOI wafer, in which XeF_2 etching removes the underlying handle silicon (Fig. 3a).[50,51] Unwinding of the coiled spirals yields an extensible system that could also achieve some degree of stretchability if bonded to an elastomeric substrate. See right frame of Figure 3a. Here, instead of out-of-plane motions, stretching is accomplished through a combination of bending of the coils of the spiral and rotation of the islands.[50,51] Another largely planar strategy uses leaf-arm springs, in which a pivoting motion provides an effective stretchability, as shown in the left frame Figure 3b.[52] (Note that although these structures are formed in a planar configuration, their response to strain involves deformations out-of-plane, in addition to in-plane rotations). The right frame of Figure 3b shows an array of interconnected islands on an inflated membrane of PDMS, as a construct that could conceivably be used for curved surface imagers similar to those described subsequently. A related approach involves planar S-shaped (i.e., serpentine) structures,[53–59] in which bending at the corners can accommodate applied strain. Figure 3c shows some examples.[53] As with the straight spring interconnects, the motion can also involve out-of-plane deformations.[30,57]

Advanced approaches combine serpentine interconnects, similar to those of Figure 3c in engineered, out-of-plane geometries using prestraining techniques and patterned bonding, similar to those of Figure 2d. Figure 4 shows an integrated circuit composed of silicon devices at bonded island locations and triple layer stacks of polymer and metal in non-coplanar, serpentine layouts as interconnects.[30] In such systems, modeling indicates that strains in the active materials can be held below ~0.1% even for applied strains larger than ~100%.[30] The interconnects accommodate these strains through combinations of bending, twisting, rotating and buckling, both in and out of the plane. Details of such systems appear in Section 3.4.

© 2010 WILEY-VCH Verlag GmbH & Co. KGaA, Weinheim
WILEY InterScience DISCOVER SOMETHING GREAT

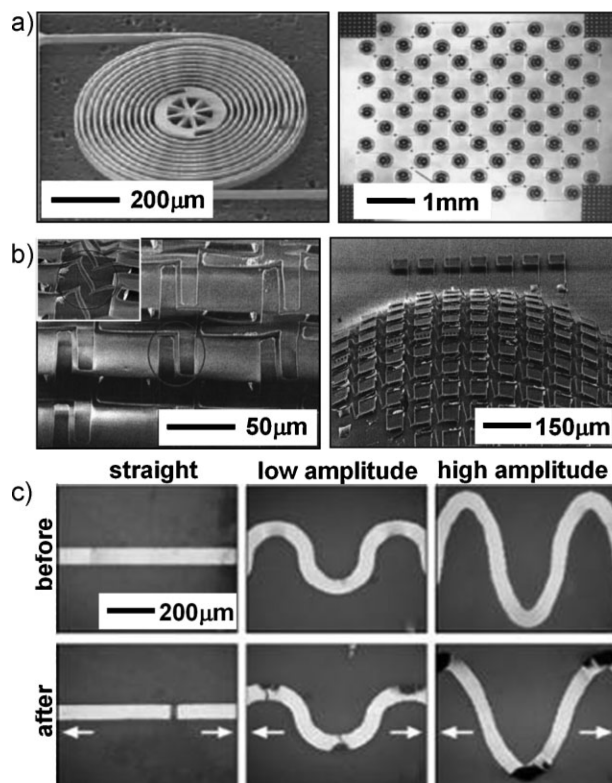

Figure 3. a) SEM image of an silicon structure etched into the shape of a spiral surrounding a central hub (left) and optical image of expanded, interconnected array of such structures (right). Reproduced with permission from ref. [51]. Copyright IEEE. b) SEM image of silicon island interconnected with straight, leaf-spring type interconnects on an elastomeric film before (right) and after (right inset) stretching, and view of the array after expansion into a dome shape by applying pressure from the back side. Reproduced with permission from ref. [52]. Copyright American Institute of Physics. c) Optical images of straight and serpentine metal lines (low- and high-amplitude structures) on an elastomeric substrate. The sequence of images on top shows the as-fabricated structures. The sequence of images on the bottom shows the same structures after application of tensile strain in the direction indicated by the arrows. The discolored regions correspond to deformations at locations of peak strain. Reproduced with permission from ref. [53]. Copyright Wiley–VCH Verlag.

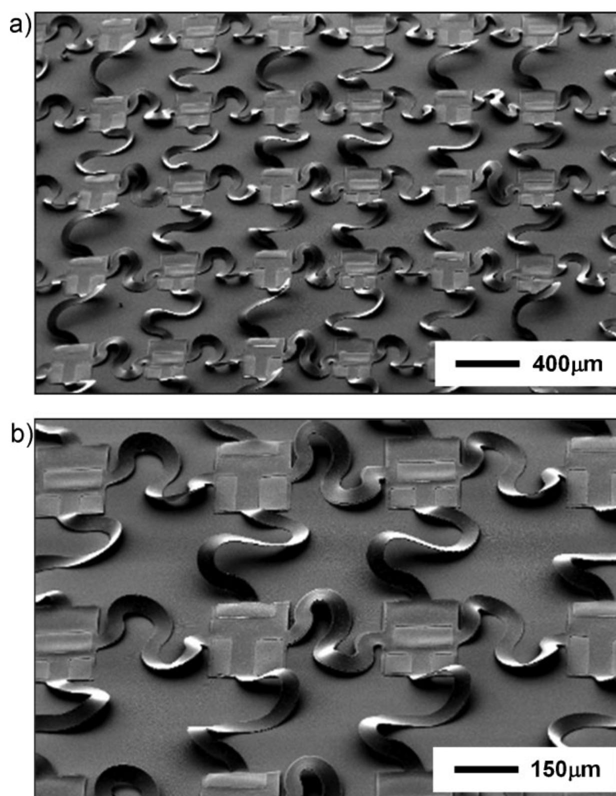

Figure 4. a) SEM image of a silicon integrated circuit composed of device islands that support transistors for CMOS inverters interconnected by non-coplanar serpentine structures consisting of trilayer stacks of polymer/metal/polymer. b) Magnified view of the circuit shown in (a). Reproduced with permission from ref. [30]. Copyright National Academy of Sciences.

3. Stretchable Electronic/Optoelectronic Systems

3.1. Stretchable Electronic and Optoelectronic Devices

The mechanics described in the previous section applies equally well to a wide range of materials, from semiconductors to conductors and insulators, both inorganic and organic. A simple device example is provided by a wavy transistor based on a single crystalline silicon nanoribbon with integrated doped and metallized regions for source and drain, a thermal SiO_2 layer for a gate dielectric and a separate metal pad for a gate.[28] Figure 5a provides a sequence of images collected from a similarly constructed pn junction diode.[28] In both cases, all processing steps to define the devices occur before transfer to PDMS. Other similar ribbon based devices include GaAs diodes and MESFETs,[33] the latter of which appears in Figure 5b. In the case of Figure 5a, the bending stiffnesses of different regions of the diode are approximately the same, such that the wavy patterns (e.g., wavelength) do not vary substantially with position along the device. By contrast, the GaAs MESFET shows large variations. In fact, both buckling modes (i.e., Fig. 1a and 1b) contribute to the response, depending on the magnitude and direction of the strain. Here, the source, drain and gate electrodes appear yellow. In the unperturbed state, the GaAs regions between the source/gate and drain/gate delaminate to form the type of bridge structures shown in Figure 1b. For relatively large compressive strain, these bridges deform in the expected way, but the metallized regions of the device also change shape, at a certain critical strain, to adopt a layout similar to Figure 1a. This combined response yields a device with electrical properties that show little change with applied strain. Solar cells and light-emitting diodes (LED) can also be constructed in this manner. Figure 5c shows an example of a red LED based on an ultrathin AlInGaP device in the shape of a ribbon, with a pattern of buckling in the mode of Figure 1a.[60] These examples illustrate that a common, and relatively simple underlying physics can be used with various devices and materials, as building blocks of more complex systems described in later sections.

© 2010 WILEY-VCH Verlag GmbH & Co. KGaA, Weinheim

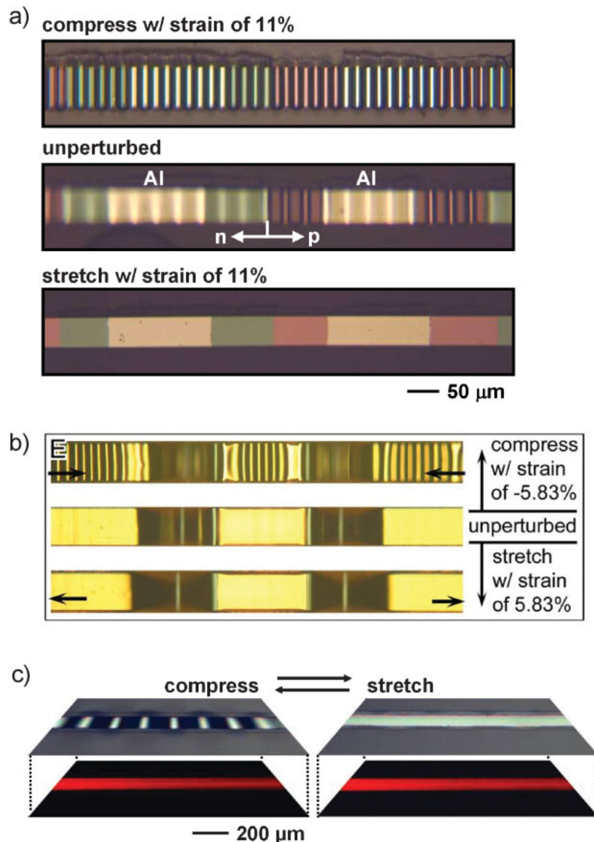

Figure 5. a) Optical microscopy images of a stretchable silicon nanoribbon pn diode on a PDMS substrate under compressive (11%; top), zero (middle) and tensile (11%; bottom) applied strains. The bright, silver regions correspond to thin (20nm) Al electrodes; the pink and green regions correspond to n (boron) and p (phosphorous) doped areas of the silicon, respectively. Reproduced with permission from ref. [28] copyright American Association for the Advancement of Science. b) Optical microscopy images of a MESFET device based on a gallium arsenide nanoribbon embedded in PDMS, under compressive (5.8%; top), zero (middle), and tensile (5.8%; bottom) applied strains. The gold regions correspond to gate (center), source and drain (left, right) electrodes. Reproduced with permission from ref. [39]. Copyright Wiley-VCH Verlag GmbH & Co. c) Optical microscopy images of a stretchable AlInGaP LED on a PDMS substrate under zero (left) and tensile (3.2%; left) applied strains. The upper and lower images in the bottom frames show illuminated, reflection mode microscopy images and microscopy images of the emission without illumination, respectively. Reproduced with permission from ref. [60]. Copyright American Association for the Advancement of Science.

3.2. Stretchable Metal Interconnects between Rigid Devices

Metal interconnects can also be formed into wavy shapes, to define stretchable wiring for separately fabricated, non-stretchable device islands.[53–59,61,62–72] This approach, which receives inspiration from Whitesides et al.[62] who observed that thin films of Au deposited onto PDMS form wavy, buckled shapes, represents the basis of some of the original work in stretchable electronics. Stretchability derives from the mechanics of such metal structures, which electrically interconnect separately fabricated, rigid active device regions that remain flat and non-stretched. In addition to the original methods of forming wavy metal lines by deposition,[66] similar morphologies can be achieved by applying strain.[63–72] In typical cases, microcracking occurs in addition to wavy structures, and both features, possibly acting in concert with the intrinsic ductility of a material like Au, all contribute to a stretchable mechanical response.[66,67] As evidence that the wave structures are not the only feature that determines the physics, interconnects prepared with 25% pre-strain can be stretched by 100% with only slight increase of the electrical resistance.[67] A different, but related type of stretchable electrode involves S-shaped serpentine patterns of metal lines fabricated on a carrier wafer and then embedded in PDMS by encapsulation and transfer.[55–59,61] Deformations of these initially planar structures occur primarily at the curved edges of the serpentines, to accommodate applied strain (e.g., Fig. 3c). By optimizing the curvature, amplitude and shape of these edges, stretchability of up to ~70% is possible.[56] Moreover, the addition of thin layers of conductive polymer on top of the metal can improve the mechanical robustness, thereby enabling stretchability to ~100% with only mild increases in electrical resistance.[54]

The conducting structures described above benefit from, but do not explicitly require, plastic deformation in the metal. Other recent work demonstrates the use of conductive liquid metal alloys and materials with liquid/solid phase transitions near room temperature (e.g., molten solders), filled into sealed, three dimensional microchannels in elastomeric materials such as PDMS.[73–76] Typically, prefabricated channels are filled with liquid alloys using pressure induced flows. The elastisticity of PDMS, combined with reversible flow in the conductor, yield a stretchable response. Deformable antennas[76] and electrical connections to light emitting diodes[74] have been demonstrated.

More sophisticated, integrated circuits can be built by connecting rigid active device components using the solid metal interconnects of described above. Figure 6a shows a demonstration of an amorphous silicon inverter that uses this design, for which stretching to strains of up to 12% is possible.[64] Here, thin wavy metal lines deposited and patterned directly on the PDMS provide interconnects between separately fabricated and assembled devices. Using a similar design, arrays of thermocouples with stretchable interconnects for monitoring body temperature have been achieved, as shown in the Figure 6b.[56] The thermocouples consist of commercially available 12-bit temperature sensor devices, each with eight contact pads on rigid silicon wafers, a decoupling capacitor, a resistor and light emitting diode as an indicator.[56] The separate fabrication and assembly of rigid device components and interconnects formed on PDMS represents an attractive approach to relatively simple systems. Devices that require distributed sensing or computation, in medium or large scale integrated formats might, however, be difficult to achieve using such procedures.

3.3. Stretchable Integrated Systems

Integrated approaches to stretchable circuits using the physics of wavy membranes (Fig. 1c) are possible. In one example, the fabrication begins with the formation of extremely bendable,

© 2010 WILEY-VCH Verlag GmbH & Co. KGaA, Weinheim
WILEY InterScience DISCOVER SOMETHING GREAT

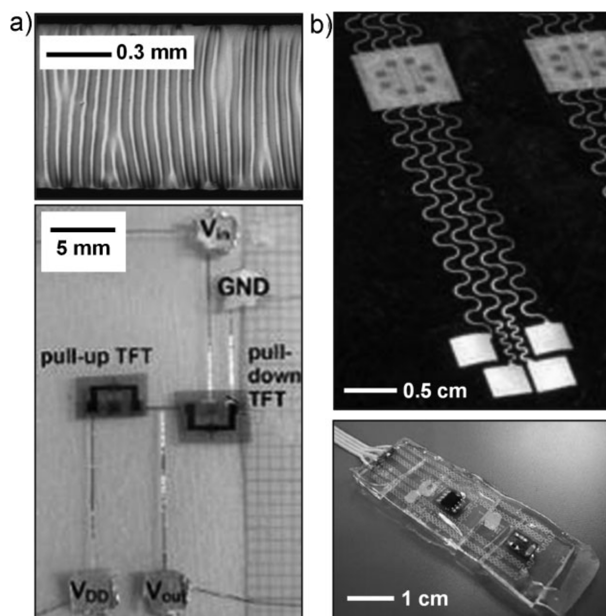

Figure 6. a) Optical microscopy image of wavy metal electrode deposited directly on a PDMS substrate (top) and image of stretchable inverter composed of non-stretchable n-type amorphous silicon TFTs, interconnected with stretchable metal lines (bottom). Reproduced with permission from ref. [64] copyright IEEE. b) Image of a set of S-shaped metal interconnects to a rigid device island, all embedded in PDMS (top) and stretchable thermocouple made of rigid semiconductor devices connected by S-shaped stretchable interconnects (bottom), also embedded in PDMS. Reproduced with permission from ref. [56]. Copyright IEEE.

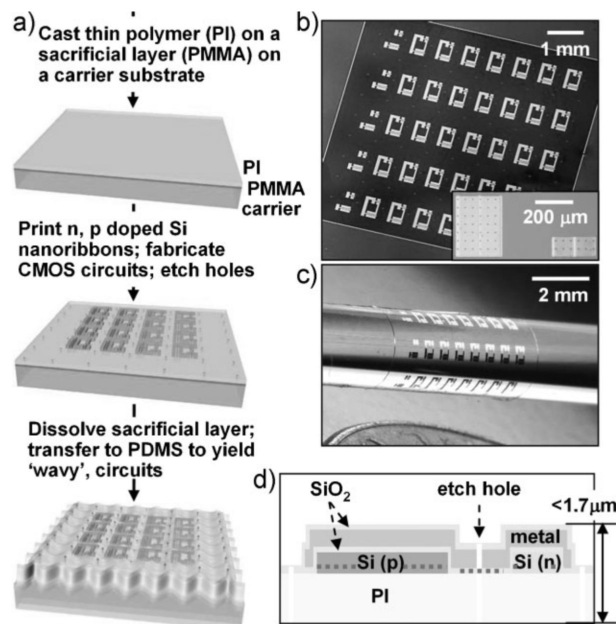

Figure 7. a) Fabrication process for CMOS circuits that exploit silicon nanoribbons in neutral mechanical plane layouts, for extreme bendability and, when integrated with an elastomeric substrate, stretchability (bottom). b) Optical image of such a circuit on a planar substrate for fabrication, and doped nanoribbons (inset). c) Circuit wrapped around a thin rod after removal from this substrate. d) Cross sectional schematic view of a pair of transistors. The dashed red line indicates, approximately, the position of the neutral mechanical plane, for different regions. Reproduced with permission from ref. [29]. Copyright American Association for the Advancement of Science.

ultrathin silicon CMOS circuits formed with the silicon near the neutral mechanical plane of a multilayer stack that includes a layer of polyimide as a substrate.[29] Bonding such circuits to biaxially stretched PDMS substrates using the chemistry described previously, followed by relaxation of the prestrain forms chip-scale wavy integrated circuits. Figure 7a provides a process flow for this case. First, a thin layer (~1.2 µm) of polyimide (PI) is spin cast on a carrier wafer coated with poly(methylmethacrylate) (PMMA). The PI and PMMA layers function as an ultrathin flexible substrate and a sacrificial layer, respectively. Transfer printing methods deliver to the PI patterned arrays of silicon nanoribbons with predefined doped regions for contacts. Next, slightly modified versions of conventional planar processing techniques, including photolithography, reactive ion etching (RIE), plasma enhanced chemical vapor deposition (PECVD) (for a gate dielectric of SiO_2), electron beam evaporation (for contact and interconnect metallization) define various layers and patterns for CMOS integrated circuits (Fig. 7b). Removing the underlying PMMA sacrificial layer with acetone releases the circuit from the carrier wafer (Fig. 7c). Bonding the circuit, after coating its backside with Cr/SiO_2, onto a biaxially pre-strained substrate of PDMS, followed by release yields an ultrathin circuit in a wavy shape with basic features similar to the much simpler system of Figure 2c. Suitable choice of thickness of the PI substrate places the neutral mechanical plane near the silicon (Fig. 7d), for enhanced bendability and, therefore, stretchability in this geometry.

Figure 8 provides images of such systems.[29] The color variations result from different reflections associated with the wavy shapes. Although the degree of deformation appears significant, the amplitudes of the waves (i.e., few micrometers) are much smaller than the characteristic wavelengths (i.e., few hundred micrometers). As a result, the maximum strains in the circuit layers are sufficiently small that good electrical properties are possible. The layouts and physics are similar to those of the uniform sheets illustrated in Figures 1c and 2c, but with more complex responses due to spatial variations in bending stiffness associated with different materials and stack thicknesses in different regions of the circuits. Although these details can be modeled at a quantitative level, from an engineering standpoint it is only important that wavy patterns are present; with them, the circuit can respond to applied strains in ways that involve small strains in the inorganic electronic materials. In addition to stretchability, such circuits are "soft", in a mechanical sense. Figure 8b illustrates this aspect, through an image of a circuit pressed downward in its center with a rigid glass rod. As is evident from this frame, the wave structures respond locally to accommodate the associated strains. Figure 9 provides some measurements of stretchable CMOS ring oscillators and differential amplifiers, at different levels of applied strain. The images reveal changes in wavelengths, amplitudes and spatial layouts of the wavy structures, as they respond to applied

© 2010 WILEY-VCH Verlag GmbH & Co. KGaA, Weinheim

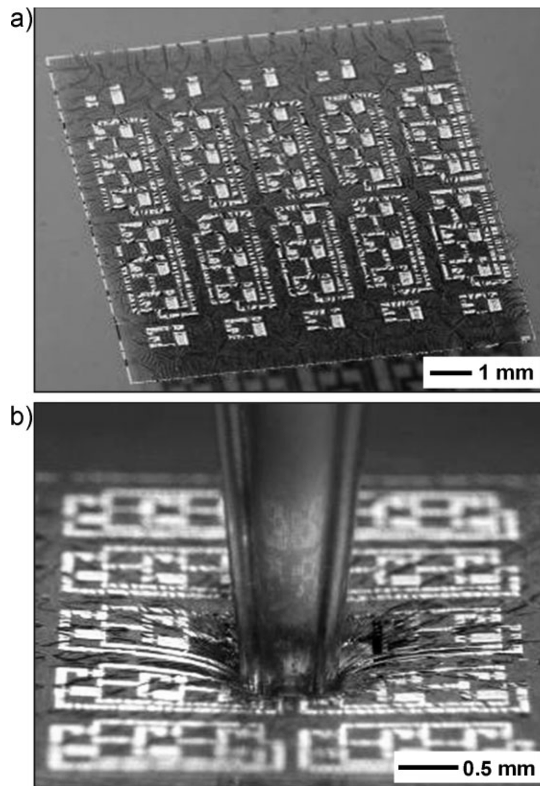

Figure 8. a) Optical image of a chip-scale silicon CMOS integrated circuit, in a ''wavy'', stretchable configuration on a substrate of PDMS. The circuit consists of ten three stage ring oscillators, five inverters, and five isolated p and n channel transistors. b) Optical image of such a circuit, mechanically deformed by application of downward force in the center with a glass rod. Reproduced with permission from ref. [29]. Copyright American Association for the Advancement of Science.

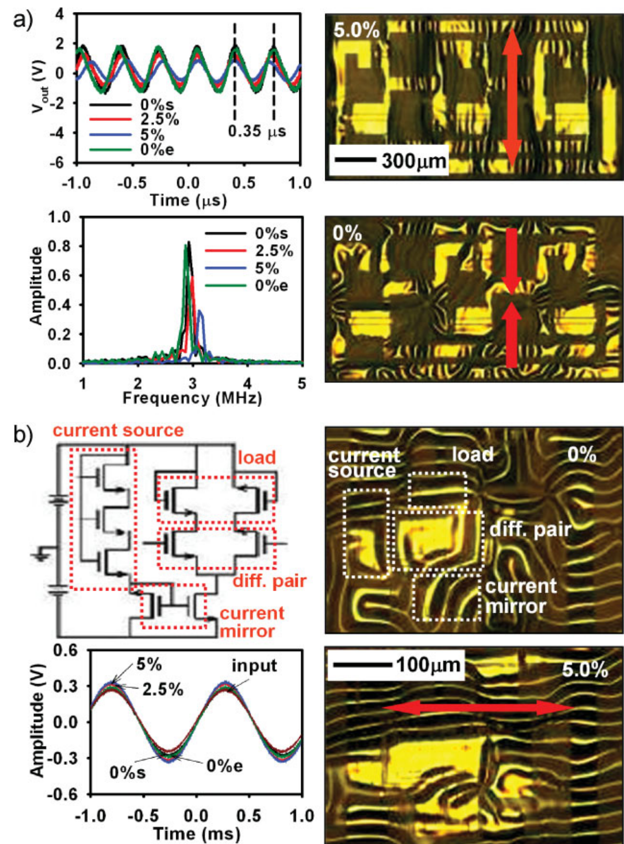

Figure 9. a) Measured time- and frequency-domain responses of a stretchable silicon CMOS ring oscillator at different applied strains. Optical images on the right show the configuration of the circuit at zero strain (bottom) and with applied tensile strain (5%) in the vertical direction (top). b) Circuit diagram of a differential amplifier and time-domain response at various strain values. Optical images on the right show the configuration of the circuit at zero strain (top) and with applied tensile strain (5%) in the horizontal direction (bottom). Reproduced with permission from ref. [29]. Copyright American Association for the Advancement of Science.

strains. The basic electronic functionality is maintained in all cases.[29]

One disadvantage of these chip-scale wavy circuits is that the active devices are not isolated from strain. As a result, stretching/compressing can cause slight changes in device performance (e.g., ring oscillator frequency in the case of Fig. 9), due to the coupling of electron and hole mobilities to strain. These effects can be seen most clearly in changes in the transfer characteristics of CMOS inverters. In a typical case, the inverter threshold voltage can change by up to 0.6 V with $\sim$10% stretching.[29] One simple method to avoid this behavior exploits mesh layouts that focus the buckling physics to regions of the circuit that have little sensitivity to strain, such as the interconnects. The result is an integrated process flow to devices that have some features in common with those in Figure 6a. Figure 10 provides an example, and an illustration of the associated fabrication steps.[77] Here, regions of the ultrathin PI substrate away from the devices and interconnects are removed by reactive ion etching, before transfer to PDMS (Fig. 10a). Three dimensional FEM simulation (Fig. 10d) and experimental results (Fig. 10b and 10c) show that this modification localizes the wavy structures to the interconnect regions, thereby isolating the silicon devices from strain. For an interconnect with the equivalent tension rigidity $\overline{Eh}$ and bending rigidity $\overline{EI}$, the wavelength is $\lambda = 2\pi(4\overline{EI}/\overline{E}_s)^{1/3}$ and the amplitude is $A = \sqrt{12(\varepsilon_{pre}/\varepsilon_c - 1)\overline{EI}/\overline{Eh}}$, where ε_{pre} is the pre-strain, $\varepsilon_c = 3(4\overline{EI}\,\overline{E}_s^2)^{1/3}/(4\overline{Eh})$ is the critical buckling strain, and $\overline{E}_s$ is the plane-strain modulus of the substrate. Strains in the interconnects and device islands obtained analytically are very small,[78] as confirmed by FEM modeling. Since the change in resistance of the metal lines with strain is negligible compared to the strain dependence of the mobilities in this silicon, this segmented structure can reduce the sensitivity of the electronics to applied strain. As an example, the variation in threshold voltage of an inverter decreases by more than five times, to $\sim$0.1 V during stretching, as shown in the Figure 10e and 10f.[77]

3.4. Non-Coplanar, Highly Stretchable Integrated Systems

The range of stretchability ($\sim$10–20%) achieved in wavy circuits of Figures 9 and 10 represent the primary limitation of that strategy.

© 2010 WILEY-VCH Verlag GmbH & Co. KGaA, Weinheim

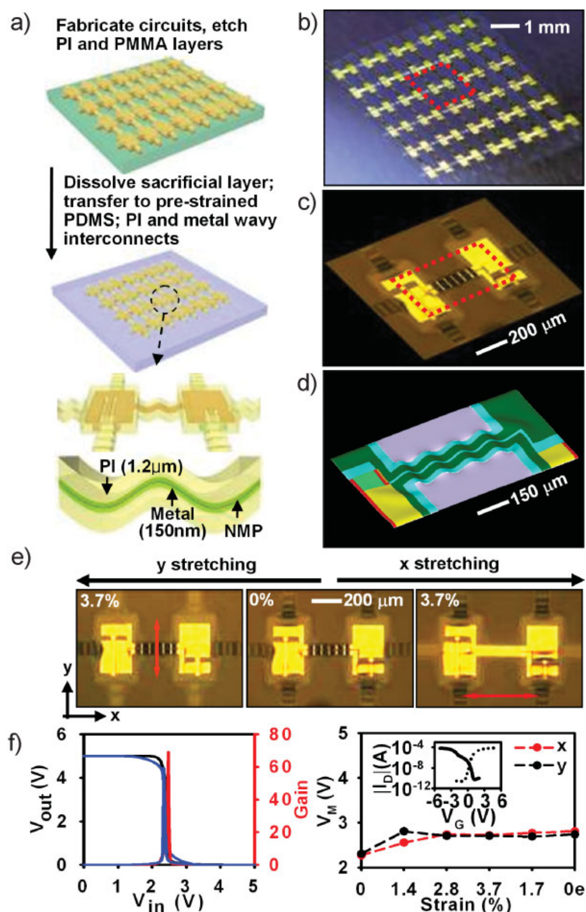

Figure 10. a) Schematic illustration of the fabrication process of silicon CMOS circuits (i.e., inverter logic gates) in a mesh geometry with stretchable, "wavy" interconnects. The bottom frame shows the use of a top layer encapsulation scheme (polyimide; PI) that locates the critical circuit elements near the neutral mechanical plane (NMP). b) Image of CMOS inverters with wavy interconnects and bridge structures. c) Magnified view of a CMOS inverter with wavy interconnects. d) Finite element simulation of the mechanics of this system, showing good agreement with experimental observation. e) Optical microscopy images of an inverter unstrained (center) and stretched in the vertical (y; left) and horizontal (x; right) directions. f) Output voltage (V_{out}) and gain as a function of input voltage (V_{in}) for a representative inverter at different applied strains. Voltage at maximum gain (V_M) as a function of strain in the x and y directions. The inset provides plots of drain current (I_D) as a function of gate voltage (V_G) for n (dashed) and p (solid) channel transistors in the inverter. Reproduced with permission from ref. [77]. Copyright American Institute of Physics.

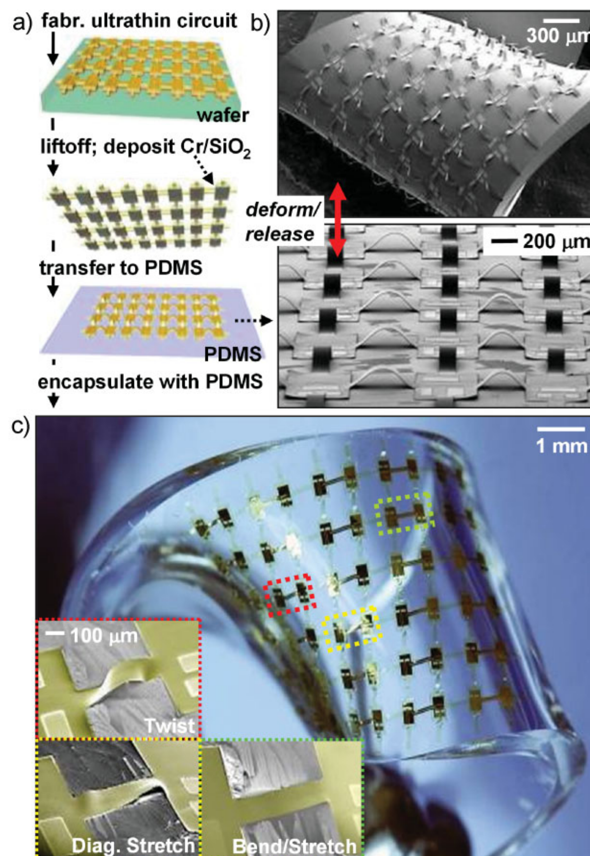

Figure 11. a) Schematic illustration of the fabrication process for stretchable electronics in non-coplanar mesh geometries on elastomeric substrates (PDMS). b) SEM images of an array of CMOS inverters that result from this process with a prestrain of 20%, in an undeformed state (bottom) and in a twisting deformation (top). c) Optical image of a similar circuit encapsulated with a layer of PDMS, stretched and twisted to highlight three different classes of deformation: diagonal stretching, twisting, and bending. The insets provide colorized SEM images for each case. Reproduced with permission from ref. [30]. Copyright National Academy of Sciences.

The concepts of Figures 1d and 2d can dramatically improve this aspect of the system. The key process steps, which build on those illustrated in Figures 7 and 10, and some images of completed circuits appear in Figure 11.[30] Selective bonding in this case can be accomplished with layers of Cr/SiO_2 deposited only onto the backsides of the islands. Release of pre-strain ε_{pre} creates arc-shaped interconnects (i.e., bridge) with amplitude $A = (2L/\pi)\sqrt{\varepsilon_{pre}/(1+\varepsilon_{pre}) - \varepsilon_c}$,[78] where $\varepsilon_c = \pi^2 h^2/(3L^2)$ is the critical buckling strain, which is very small because the interconnect thickness h is much smaller than the initial length L. The maximum strain in the interconnect, $(\varepsilon_{interconnect})_{\max} = 2\pi(h/L)\sqrt{\varepsilon_{pre}/(1+\varepsilon_{pre})}$, is much smaller than the pre-strain because of the small ε_c. The maximum strain in the island is given by $(\varepsilon_{island})_{\max} = (\varepsilon_{interconnect})_{max} \cdot Eh^2/(\overline{E}_{island}h^2_{island})$, which is negligibly small for interconnect thickness h much smaller than the island thickness h_{island}, where E is the Young's modulus of interconnect, and $\overline{E}_{island}$ is the plane-strain modulus of the island. The increased stretchability provided by the arc-shaped interconnection bridges provides reversible, elastic responses to deformations of nearly any type. Figure 11c provides some optical and SEM images that highlight responses to various applied forces. The complex deformation mode illustrated in Figure 11 consists of the superposition of several basic motions, such as horizontal and diagonal stretching or twisting. For each deformation, the corresponding strain absorbed through motions of the bridges avoids any significant effect on the islands. A neutral mechanical plane design for the metallization in the bridges minimizes the strain that they experience. All of these effects can be captured with finite element modeling (FEM) analysis as shown in Figure 12. In the strain distribution, red and

© 2010 WILEY-VCH Verlag GmbH & Co. KGaA, Weinheim

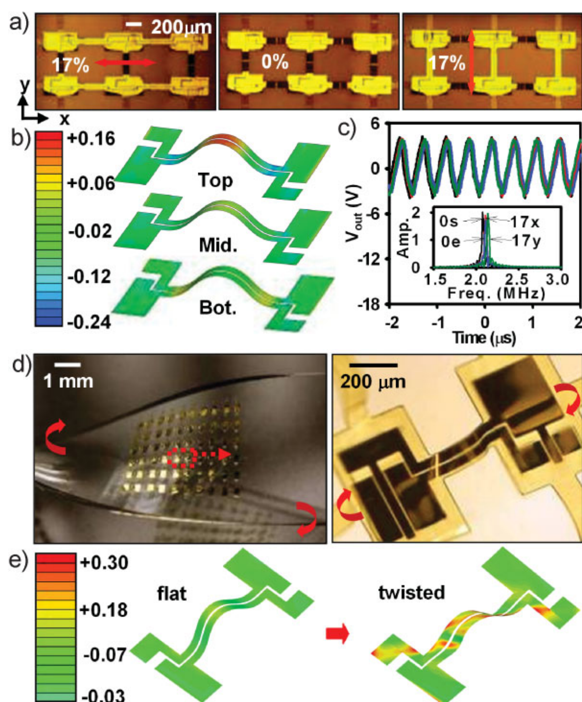

Figure 12. a) Optical images of stretchable, 3-stage CMOS ring oscillators with non-coplanar mesh designs, stretched along the interconnects (*x* and *y*). b) Finite element modeling of the strain distributions at the top surface of the circuit (top) and at the midpoint of the metal layer of the interconnects (middle) and at the bottom surface (bottom). The labels for the legend give the strain magnitudes in percent. c) Time- and frequency- (inset) domain electrical characteristics of the oscillators in the different strain configurations. 0s and 0e refer to 0% strains at the start and end of the testing, respectively; 17*x* and 17*y* refer to 17% tensile strains along the *x* and *y* directions indicated in (a), respectively. d) Optical images of an array of stretchable CMOS inverters with a non-coplanar mesh design, in a twisted configuration (left) and magnified view of a single inverter (right). e) Finite element modeling of the mechanics of this type of twisting deformation. The labels for the legend give the strain magnitudes in percent. Reproduced with permission from ref. [30]. Copyright National Academy of Sciences.

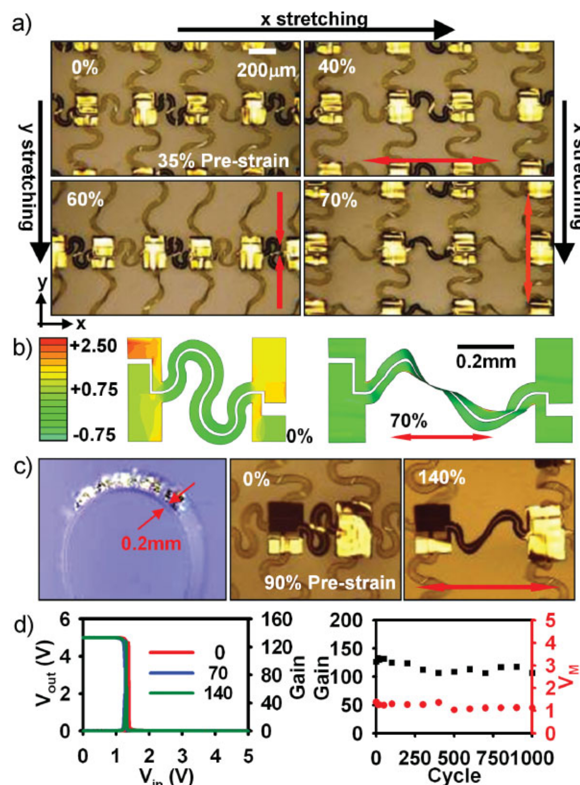

Figure 13. a) SEM image of an array of stretchable CMOS inverters with non-coplanar mesh designs and serpentine interconnects (left) and magnified view (right). b) Optical images of stretching tests in the x and y directions. The labels for the legend give the strain magnitudes in percent. c) Finite element modeling of the mechanics before (35% prestrain) and after (70% applied strain) stretching. d) Arrays of inverters on a thin PDMS substrate (0.2 mm thick) (left) and images in unstretched (middle; 90% prestrain) and stretched (right; 140% tensile strain) configurations. e) Plot of V_{out} and gain as a function of V_{in} for a representative inverter under stretching (left) and similar plot of gain (left). Plot of gain and voltage at maximum gain (V_M) for a similar device as a function of stretching cycles (right). Reproduced with permission from ref. [30]. Copyright National Academy of Sciences.

blue regions correspond to tensile and compressive strains, respectively; green represents areas with nearly zero strain.

Bending strains in the bridges often limit the range of stretchability. As shown by the above expression for maximum strain, decreasing their thickness, or increasing their lengths can reduce these strains. This latter strategy can be implemented, for example, with bridges that connect opposite, rather than nearest, edges in adjacent islands.[79] Further improvements are possible by replacing the straight, non-coplanar bridges with structures that have serpentine shapes, as outlined in Figure 4.[30] The serpentine bridges can provide much larger stretchability than the straight ones due to two major advantages: i) they can accommodate much larger pre-strain than straight ones due to their much longer lengths; ii) when the applied strain reaches the pre-strain, serpentine bridges can be further stretched due to the buckling modes associated with the serpentine geometry; the straight geometries cannot. Figure 13a presents optical microscope images of serpentine bridges at different applied strains. Upon release of pre-strain, the bridges are compressed and move out of the plane of the circuit, as shown in the left top frame of Figure 13a. For applied strains similar the pre-strain (e.g., 40% applied strain for 35% pre-strain; right top frame of Fig. 13a), the serpentines return to a geometry close to their original, as-fabricated state. Unlike straight bridges, however, the serpentines can continue to move, through rotations and out-of-plane motions, for applied strains larger than the pre-strain to enable much larger stretching than would otherwise be possible.[30,58,72,80] See bottom frames of Figure 13a. The strain distributions evaluated by FEM simulation appear in Figure 13b. With increased pre-strain, the stretchability can be increased once again, to over ~100%. In the example of Figure 13c, a thin substrate of PDMS (~0.2 mm) facilitates application of prestrains and applied strains in this relatively large range: ~90% pre-strain, and maximum stretchability of ~140%. Experimental results indicate reversible behavior even at these levels of deformation. Figure 13d shows the electrical characterization results for 1000 times repetitive stretching tests.

The non-coplanar layouts of these serpentine structures are critically important to their operation. Figure 14 compares

© 2010 WILEY-VCH Verlag GmbH & Co. KGaA, Weinheim

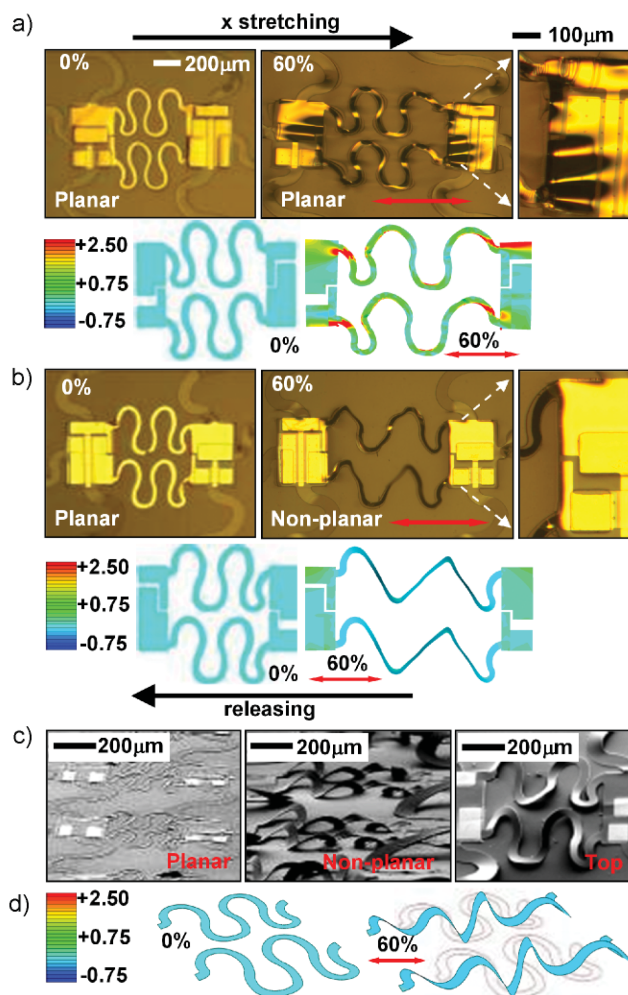

Figure 14. Optical microscopy images (upper) and maximum principal strain distributions computed by finite element modeling (lower) for CMOS inverters with serpentine interconnects in a) coplanar and b) non-coplanar layouts. c) SEM images before (left) and after (center and right) applying strain for the non-coplanar design and corresponding finite element modeling (d). In all cases, the labels for the legends give the strain magnitudes in percent.

coplanar and non-coplanar configurations.[80] For the coplanar case, all bridge and island regions are attached to the bottom PDMS substrate through covalent bonding between PDMS and SiO_2 deposited on the backsides of the circuits. For the non-coplanar case, only the island regions are bonded in this manner. To facilitate comparison, pre-strain is not used, such that the initial strain distributions are the same, as shown in left frames of Figure 14a and 14b. For applied strains of 60%, the bridges in the coplanar case remain bonded to the PDMS substrate, while certain portions of the bridges in the non-coplanar case move up, out of the plane. Figure 14c shows this latter behavior in SEM images. The left frame (60° tilted) corresponds to zero applied strain; the center (60° tilted) and right (top view) frames correspond to 60% tensile strain. Restricted movement due to bonding to the PDMS in the coplanar layout results in higher strains than in the non-coplanar configuration. As a result, cracks and wrinkles inside the island region are evident in the coplanar devices but not in the non-coplanar, at large applied strains. See center and right images of Figure 14a and 14b. The strain distributions and maximum principal strain values calculated by FEM analysis confirm these experimental observations (bottom frames of Fig. 14a and 14b). In particular, the maximum principal strain under ~60% external strain for coplanar and non-coplanar structure is 6.8% and 0.18%, respectively.[80] Figure 14d shows tilted views of the FEM simulation results for the non-coplanar structure before and after applying strain, to highlight the out of plane configuration. In these systems, additional improvements are possible by extending the lengths of the serpentines or reducing their widths or thicknesses.[80] Such design strategies must be balanced, of course, by electrical requirements on the circuits.

3.5. Stretchable Encapsulated Systems

All electronic systems require encapsulation to provide mechanical and environmental protection for use in any realistic system. For many cases described here, rigid organic or inorganic layers can be deposited as thin films on devices or interconnects prior to their integration with elastomeric supports. The entire systems, however, can benefit also from a top layer to embed the circuits in elastomer, above and below. For designs that rely on out-of-plane motion, the mechanical loading effects of this top encapsulation layer are important to understand, particularly for those that use extreme non-coplanar layouts for large stretchability. Generally, this layer should offer elastic response to large strains, and it should also have a low modulus to minimize mechanical constraints on the motion of the circuit structures as they accommodate applied strains. To reveal quantitatively the effects, inverter circuits with straight arc-shaped bridge structures and encapsulated with PDMS formulations that have different moduli can be compared.[80] Stretching to the point of failure in the interconnect metal, as shown in Figure 15a, represents the basis of one such comparison. In Figure 15b, the modulus of the encapsulating PDMS in the right and center frame is 1.8 MPa and 0.1 MPa, respectively. A control sample without encapsulation (left frame) provides a point of comparison. With ~60% pre-strain, the unencapsulated device can be stretched to ~59% without failure, as expected. The systems encapsulated using PDMS with moduli of 0.1 MPa and 1.8 MPa, failed at 55% and 49%, respectively. The range of observed failure strains is ~2%. Combined with the amplitude difference in Figure 15c, these results reveal differences between each encapsulation. The responses in these cases compare favorably to analytical and FEM simulation, as demonstrated by agreement between measured and calculated amplitudes of the bridges at various levels of applied strain (top frames and bottom left frame of Fig. 15c). The theory also provides an estimate for the maximum stretchability in these three cases.[80] The results match intuition and experiment, thereby providing a basis for design rules on the selection of encapsulants.

3.6. Stretchable, Strain Isolated Systems

Stretchable electronic devices provide the opportunity for integration on diverse substrates, with wide ranging mechanical

WILEY InterScience DISCOVER SOMETHING GREAT
© 2010 WILEY-VCH Verlag GmbH & Co. KGaA, Weinheim

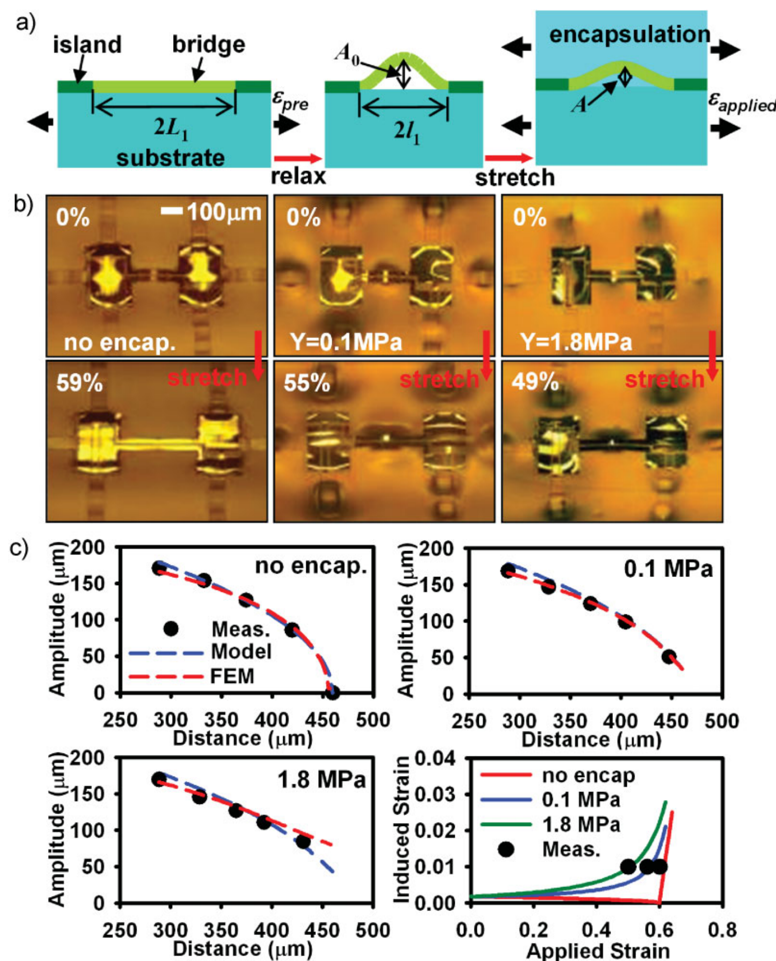

Figure 15. a) Schematic illustration of stretching test procedures and key dimensional variables for an encapsulated, straight non-coplanar interconnect. b) Optical microscopy images of the structure for the cases of zero strain (top) and maximum stretching before visible cracking (bottom) for the cases of no encapsulation (left), soft encapsulation (0.1 MPa, center) and hard encapsulation (1.8 MPa, right). c) Amplitude of the non-coplanar interconnect as a function of distance between the two islands determined by experiment, analytical modeling and finite element modeling (FEM) for the three encapsulation scenarios. The right bottom graph shows the maximum induced strain in the interconnect materials estimated by theoretical modeling as a function of strain applied to the system. The data points correspond to experimentally estimated applied strains required for fracture.

properties. Fabric, vinyl, leather and paper, as examples, represent materials with proven utility in various areas of application. An ability to integrate high-performance inorganic electronics on such surfaces could, therefore, be of interest. These materials are not stretchable, to any significant degree, but they are incompatible with devices that offer simple flexibility because they can accommodate folding and shearing type deformations. A key challenge for integration of stretchable circuits that use, for example, non-coplanar mesh designs is to reduce the potential for stress concentrations near device islands. One method uses low modulus, elastomeric adhesives, such as PDMS via bonding chemistries described previously, to isolate these devices from strains in the underlying substrate.[81] Qualitatively, such a layer provides weak mechanical coupling, such that bending the substrate leads to only relatively small bending at the islands, for example. As a result of this mechanics, bend induced strains in the electronic materials can be much lower than would otherwise be expected. Figure 16 provides an example of an array of silicon inverters in a serpentine mesh geometry mounted on a piece of fabric by use of a thin film of PDMS as an adhesive and strain isolation layer. Such circuits are compatible with random deformations of the fabric. The key physics appears in Figure 16b, which shows the computed ratio of the surface strain for a strip of silicon (300 nm thick) with and without a layer of PDMS on a sheet of plastic (100 μm thick), as a function of the width of the silicon and the thickness of the PDMS. The isolation efficiency increases with increasing PDMS thickness and decreasing silicon width, as might be expected. For parameters comparable to those of Figure 16a, the isolation provides ∼100× reduction in strain, thereby enabling extreme degrees of bending even without ultrathin layouts or neutral mechanical plane designs. Figure 17 provides similar examples for the cases of circuits on vinyl and leather gloves, and on a sheet of paper.[81] Experiments show that 1000 cycles of bending at the knuckle position and folding cause little change in electrical properties, as shown for the case of paper in Figure 17d. The inverter threshold voltage changes by less than ±0.4 V and the gain value by less than ±15%. Applications such as these might provide opportunities for stretchable, strain isolated circuits in which the final device itself is not stretchable, similar to examples described in the next two sections.

3.7. Stretchable Routes to Curvilinear Systems

Curved focal plane arrays and other envisioned applications require electronic/optoelectronic systems that conformally integrate with curvilinear surfaces. Stretchable systems enable this outcome in a general way that avoids the difficult technical challenges associated with device processing on such surfaces. One approach to integration begins with the formation of a thin, elastomeric membrane that has the surface geometry of the target, curvilinear substrate.[79,82–85] Mounting this element a radial tensioning stage allows it to be stretched into the flat shape of a drumhead. In this geometry, the element can receive a circuit separately fabricated on a planar substrate, in the ultrathin or mesh layouts described previously. Releasing the tension causes the element to relax elastically back to its original shape, carrying the circuit along with it via induced buckling or formation of non-coplanar bridges. This process accomplishes a geometrical transformation from planar to curvilinear layouts. In a final step, the structure is transferred to the target substrate. Figure 18 shows the use of these approaches to form a non-coplanar stretchable circuit conformally wrapped onto the fingertip of a mannequin hand, at various viewing angles and levels of magnification. Experimental and theoretical details of this and other related examples appear elsewhere.[79]

© 2010 WILEY-VCH Verlag GmbH & Co. KGaA, Weinheim

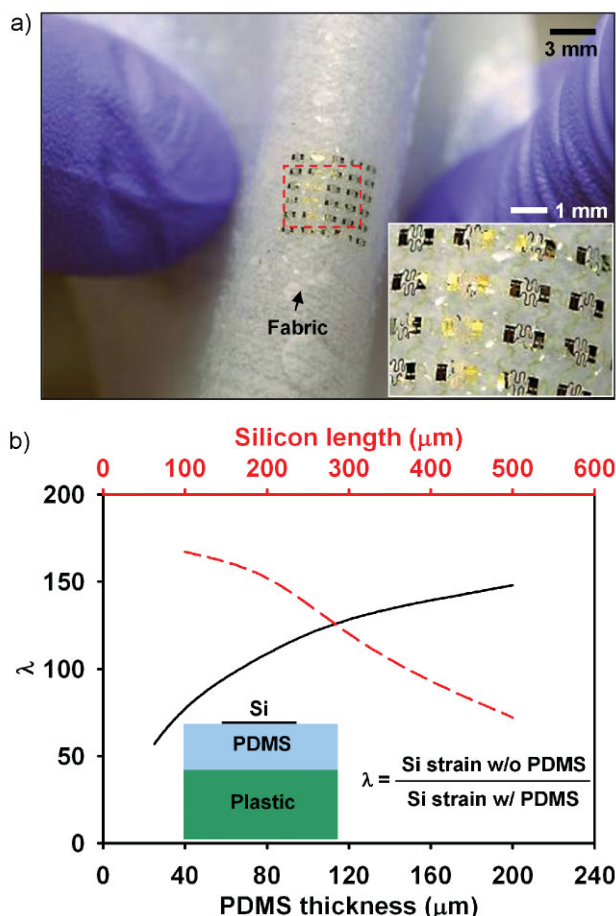

Figure 16. a) Optical image of a stretchable circuit integrated on a fabric substrate coated with a thin layer of PDMS (top) and magnified view (top right). The bottom left frame provides a schematic illustration. b) Computed ratio of the surface strain (λ) in the silicon of the system schematically illustrated in the inset, for the cases with and without the PDMS layer, as a function of thickness of the PDMS (black solid line) and length of the silicon (red dotted line; PDMS thickness is 100 μm for this case). The results show that the PDMS provides strain isolation for the silicon, with increasing effectiveness as the silicon length decreases and the PDMS thickness increases.

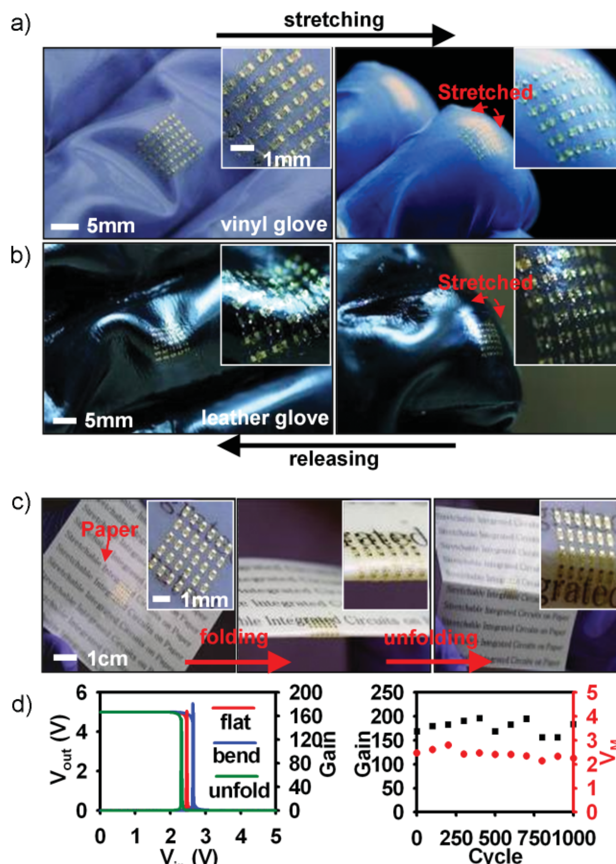

Figure 17. Optical images of stretchable CMOS circuits on finger joints of vinyl (a) and leather (b) gloves in released (left) and stretched (right) states. The insets provide magnified views. c) Optical images of CMOS inverters on paper, in flat (left), folded (center) and unfolded (right) states. Magnified views appear in the insets. d) Plot of V_{out} and gain as a function of V_{in} for a representative inverter in flat, folded, and unfolded states (left). Plot of gain and voltage at maximum gain (V_M) for a similar device as a function of folding cycles (right).

4. Application Examples

4.1. Hemispherical Electronic Eye Cameras

Digital imagers that exploit bio-inspired designs offer advantages over conventional, planar devices.[86,87] For example, photodetector arrays on hemispherical surfaces provide analogs to retinas in mammalian eyes. With simple imaging optics, such layouts achieve improved field of view, illumination uniformity and lower aberrations compared to planar systems.[52,87] As mentioned in Section 3.7, electronics/optoelectronics in non-planar geometries can be difficult to achieve, due to the intrinsically planar nature of established fabrication techniques. Past and current work in hemispherical images range from the use of unconventional methods and materials for device processing directly on curved surfaces,[88–91] to techniques for self-assembly of device blocks[92–94] to means for deforming flat or structured silicon wafers or films.[50–52,95–98] An approach that uses the methods described in previous sections recently yielded the first working hemispherical electronic eye type cameras.[82–85] These devices (Fig. 19) also achieved sufficient resolution to demonstrate the key optical effects, and to compare with planar designs.[82] A magnified view and circuit diagram of an array of silicon photodetectors and blocking diodes to facilitate passive matrix readout appear in the top and right bottom frames of Figure 19a, respectively. Integrating this imager with a printed circuit board (Fig. 19b) and a simple plano-convex lens mounted on a hemispherical shell yields a working camera in which a computer provides coordinated addressing of the photodetectors for image capture. Figure 20 shows representative examples, in grey scale and color, respectively. In each case, the curved image recorded directly from the camera appears above, with a planar projection below. The actual objects appear as small insets on the right. The bottom frame provides an example of an image collected from a camera with the curvature of a paraboloid,[84] which better matches the optical requirements than a hemispherical layout.

© 2010 WILEY-VCH Verlag GmbH & Co. KGaA, Weinheim

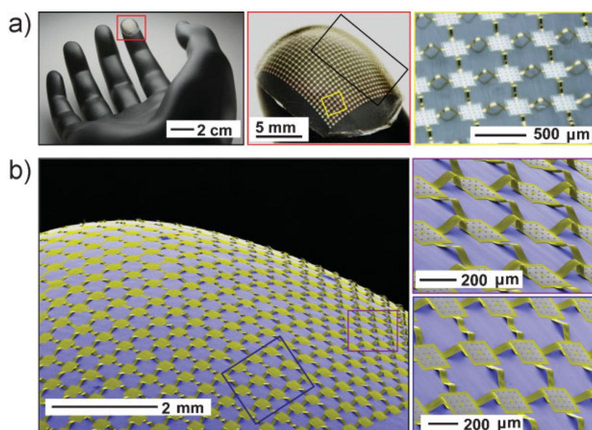

Figure 18. a) Photographs of a stretchable circuit with a non-coplanar mesh design transferred onto the tip of a finger on a plastic model of a human hand. The center frame corresponds to the red box in the left frame. The right frame corresponds to the yellow box in the center frame, collected using a scanning focal technique. b) Colorized SEM image of the region near the black box in the center frame of (a). The right frames show images of the regions indicated by boxes in (b). The gray, yellow, and blue colors correspond to silicon, polyimide, and PDMS, respectively.

These and other advanced designs that use tiled arrays of pixels,[83] as a route to high-resolution imagers, are compatible with the general approaches to curvilinear systems summarized here.

4.2. Deformable Lighting Systems

Light-emitting diodes (LEDs) in addressable arrays that exploit stretchable concepts outlined previously yield conformal lighting/display devices. Application possibilities range from ergonomic or aesthetic designs in automotive lighting or consumer electronics, to flexible display or instrumentation gauging, to imaging devices for biomedical uses. Recent work on ultrathin inorganic LEDs in microscale geometries.[60] provides a path to such systems with opportunities different than those afforded by organic LEDs. Configuring these types of LEDs in interconnected mesh structures and bonding them to elastomeric substrates yields lighting/display elements with the features of the electronic circuits discussed previously. Figure 21 shows picture of a representative device, consisting of 256 AlInGaP LEDs, each with a thickness of only 2.5 µm. Straight arc-shaped interconnects formed using procedures similar to those illustrated in Figure 11 can accommodate applied strains in the range of tens of percent. A slab of PDMS provides the substrate. Passive matrix addressing schemes enable operation of this collection of LEDs in a display mode. (In Fig. 21, only a small fraction of the LEDs are lit, to demonstrate the addressing capability.) The devices show negligible changes in operating characteristics throughout the range of strains induced by the deformation shown here. In particular, calculation shows that for strains of 24%, as defined by the change in separation between inner edges of adjacent device islands, the maximum strains in the LEDs and their quantum well regions are $<0.2\%$ and $<0.03\%$, respectively. The computed change in emission wavelength associated with this strain is less than $\sim$0.3 nm.

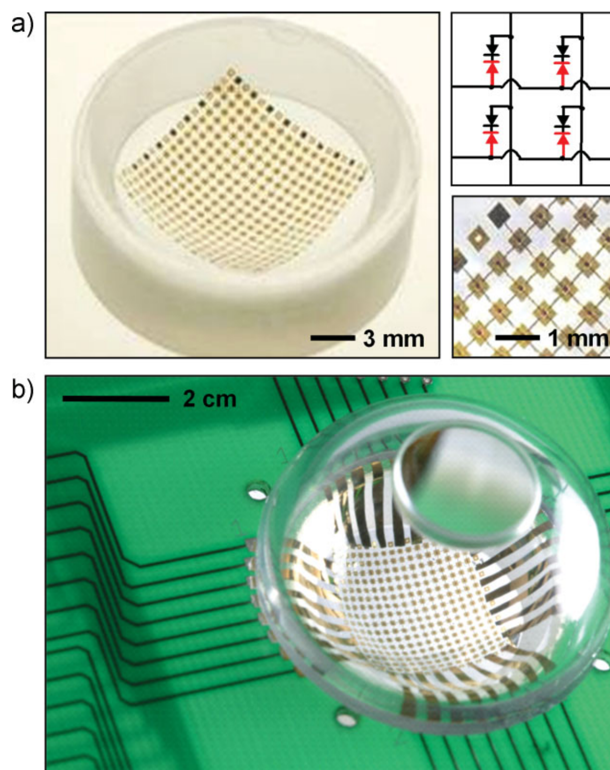

Figure 19. a) Photograph of a stretchable array of photodetectors (PDs) and blocking diodes (BDs), in a non-coplanar mesh design conformally wrapped onto the concave surface of a hemispherical glass substrate. The lower right frame shows an optical microscopy image of part of the array. The upper right frame provides a circuit diagram showing the BDs (black), PDs (red) and electrode crossovers (arcs) in a 2×2 section of the system. b) Photograph of a hemispherical focal plane array like the one shown in (a), mounted on a printed circuit board (green), with external connection to a computer (not shown) through a ribbon cable and integrated with a transparent (for ease of viewing) hemispherical cap that supports a simple, single component imaging lens. Reproduced with permission from ref. [82]. Copyright Nature Publishing Group.

5. Conclusion and Outlook

Work summarized here provides convincing demonstrations that rigid, brittle and planar inorganic materials can yield devices, circuit components and complete, integrated systems with surprising mechanical and geometrical properties, from exceptionally high levels of flexibility, to elastic responses to large strain deformations, to effective moduli comparable to a rubber band, in complex, curvilinear shapes. The designs rely critically on extreme forms of heterogeneous integration, including not only diverse classes of semiconductor materials (e.g., Si, GaN, GaAs, and others) but also unusual substrates (e.g., plastic, elastomers and others), spanning mechanical properties from the ultrahard (e.g., moduli approaching 1 TPa, for diamond, SWNTs and graphene) to the ultrasoft (e.g., 0.1 MPa for certain formulations

© 2010 WILEY-VCH Verlag GmbH & Co. KGaA, Weinheim

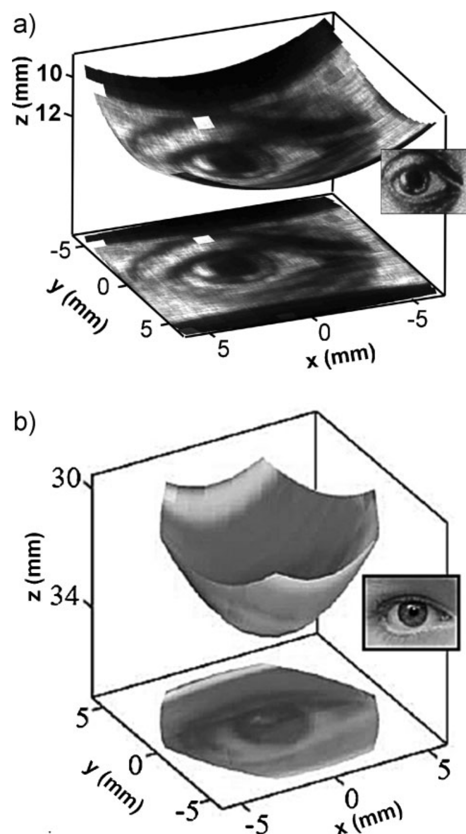

Figure 20. a) Image of a drawing of an eye, captured using a hemispherical electronic eye camera. The top part of this frame corresponds to the image as collected from the camera, rendered on a hemispherical surface that matches the curvature of the photodetector array. The bottom corresponds to a planar projection. The small image on the right represents the actual object. b) Similar image of a color picture of an eye, captured using a paraboloid camera by combining separate grey scale images collected with red, green and blue filters. Reproduced with permission from ref. [82]. Copyright Nature Publishing Group.

of PDMS). The associated research challenges involve a wide range of interesting topics in materials science, from fundamental aspects of micro/nanomechanics, charge transport and the coupling of the two, to growth and processing, to aspects of adhesion and interface science, to thermal management, thin film optics, light coupling and related. The field also has broad and deep interdisciplinary content, as evidenced by published researchers with department affiliations including not only materials science, but also chemistry, physics, mechanical engineering, electrical engineering, civil engineering and even mathematics.[99]

From an engineering perspective, systems of this type have the potential to influence the designs and application aspects of nearly all existing electronic/optoelectronic technologies. More important, they also open up completely new possibilities. Of the many potential areas, some of the most compelling are, in our view, in biomedical devices that address important problems in human health. Recent work in this direction using passive stretchable electrodes for research applications[100,101] will rapidly expand into fully integrated, biocompatible electronic systems for

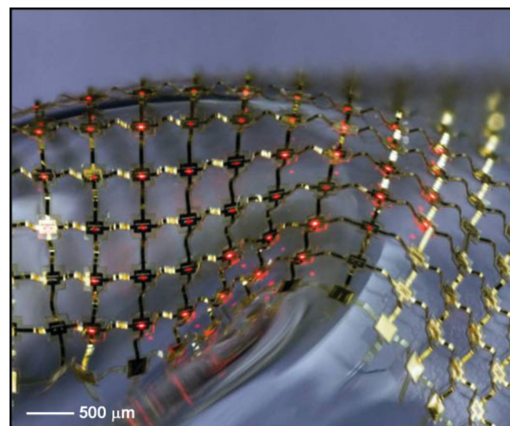

Figure 21. Passive matrix, stretchable display based on an array of inorganic LEDs in a non-coplanar mesh configuration on a PDMS substrate. The picture was collected with an automated camera system that combines images captured at different focal depths to provide a sharp, composite image. Reproduced with permission from ref. [60]. Copyright American Association for the Advancement of Science.

clinical use.[102] Heterogeneous designs in these devices will facilitate solutions to well-known materials challenges in avoiding unwanted immune responses. Soft, elastic mechanical properties and curvilinear layouts will enable, for the first time, forms that provide both mechanical modulus and shape matching to biological tissues. The diverse and interesting range of fundamental problems in materials science, the challenging topics in device and system engineering and the large, varied application spaces with important societal implications represent strong motivating forces for continued and expanded efforts in this field.

Acknowledgements

We thank T. Banks for help of in processing at the Frederick Seitz Materials Research Laboratory. This material is based upon work supported by the National Science Foundation under grant ECCS-0824129, NSFC, and the U.S. Department of Energy, Division of Materials Sciences under Award No. DE-FG02-07ER46471, through the Materials Research Laboratory and Center for Microanalysis of Materials (DE-FG02-07ER46453) at the University of Illinois at Urbana-Champaign. John A. Rogers acknowledges support from a National Security Science and Engineering Faculty Fellowship.

Received: October 5, 2009
Published online: January 25, 2010

[1] G. Moore, *Electronics* **1965**, *38*, 114.
[2] International Technology Roadmap for Semiconductors (ITRS) 2007, http://www.itrs.net/Links/2007ITRS/Home2007.htm (last accessed November 2009).
[3] M. J. Powell, *IEEE Trans. Electron Devices* **1989**, *36*, 2753.
[4] R. H. Reuss, B. R. Chalamala, A. Moussessian, M. G. Kane, A. Kumar, D. C. Zhang, J. A. Rogers, M. Hatalis, D. Temple, G. Moddel, B. J. Eliasson, M. J. Estes, J. Kunze, E. S. Handy, E. S. Harmon, D. B. Salzman, J. M. Woodall, M. A. Alam, J. Y. Murthy,

© 2010 WILEY-VCH Verlag GmbH & Co. KGaA, Weinheim

S. C. Jacobsen, M. Olivier, D. Markus, P. M. Campbell, E. Snow, *Proc. IEEE* **2005**, *93*, 1239.
[5] R. H. Reuss, D. G. Hopper, J.-G. Park, *MRS Bull.* **2006**, *31*, 447.
[6] G. Gustafsson, Y. Cao, G. M. Treacy, F. Klavetter, N. Colaneri, A. J. Heeger, *Nature* **1992**, *357*, 477.
[7] C. C. Wu, S. D. Theiss, G. Gu, M. H. Lu, J. C. Sturm, S. Wagner, S. R. Forrest, *IEEE Electron Device Lett.* **1997**, *18*, 609.
[8] J. A. Rogers, Z. Bao, K. Baldwin, A. Dodabalapur, B. Crone, V. R. Raju, V. Kuck, H. Katz, K. Amundson, J. Ewing, P. Drzaic, *Proc. Natl. Acad. Sci. USA* **2001**, *98*, 4835.
[9] J. A. Rogers, *Science* **2001**, *291*, 1502.
[10] T.-W. Lee, J. Zaumseil, Z. Bao, J. W. P. Hsu, J. A. Rogers, *Proc. Natl. Acad. Sci. USA* **2004**, *101*, 429.
[11] Stephen R. Forrest, *Nature* **2004**, *428*, 911.
[12] G. H. Gelinck, H. Edzer, A. Huitema, E. Veenendaal, E. Cantatore, L. Schrijnemakers, J. B. P. H. Putten, T. C. T. Geuns, M. Beenhakkers, J. B. Giesbers, B.-H. Huisman, E. J. Meijer, E. M. Benito, F.J.T, A. W. Marsman, B. J. E. Rens, D. M. Leeuw, *Nat. Mater.* **2004**, *3*, 106.
[13] S. Lee, B. Koo, J.-G. Park, H. Moon, J. Hahn, J. M. Kim, *MRS Bull.* **2006**, *31*, 455.
[14] J. Roncali, P. Leriche, A. Cravino, *Adv. Mater.* **2007**, *19*, 2045.
[15] C. Reese, Z. Bao, *Mater. Today* **2007**, *10*, 20.
[16] A. C. Mayer, S. R. Scully, B. E. Hardin, M. W. Rowell, M. D. McGehee, *Mater. Today* **2007**, *10*, 28.
[17] L. Xiao, Z. Chen, C. Feng, L. Liu, Z.-Q. Bai, Y. Wang, L. Qian, Y. Zhang, Q. Li, K. Jiang, S. Fan, *Nano Lett.* **2008**, *8*, 4539.
[18] Q. Cao, H.-S. Kim, N. Pimparkar, J. P. Kulkarni, C. Wang, M. Shim, K. Roy, M. A. Alam, J. A. Rogers, *Nature* **2008**, *454*, 495.
[19] K. S. Kim, Y. Zhao, H. Jang, S. Y. Lee, J. M. Kim, K. S. Kim, J.-H. Ahn, P. Kim, J.-Y. Choi, B. H. Hong, *Nature* **2009**, *457*, 706.
[20] T. Sekitani, Y. Noguchi, K. Hata, T. Fukushima, T. Aida, T. Someya, *Science* **2008**, *321*, 1468.
[21] T. Sekitani, H. Nakajima, H. Maeda, T. Fukushima, T. Aida, K. Hata, T. Someya, *Nat. Mater.* **2009**, *8*, 494.
[22] T. Someya, *Adv. Mater.* in press.
[23] H. Jiang, D.-Y. Khang, J. Song, Y. Sun, Y. Y. Huang, J. A. Rogers, *Proc. Natl. Acad. Sci. USA* **2007**, *104*, 15607.
[24] J. Song, H. Jiang, W. M. Choi, D. Y. Khang, Y. Huang, J. A. Rogers, *J. Appl. Phys.* **2008**, *103*, 014303.
[25] J. Song, H. Jiang, Y. Huang, J. A. Rogers, *J. Vac. Sci. Technol. A* **2009**, *27*, 1107.
[26] A. J. Baca, J.-H. Ahn, Y. Sun, M. A. Meitl, E. Menard, H.-S. Kim, W. M. Choi, D.-H. Kim, Y. Huang, J. A. Rogers, *Angew. Chem. Int. Ed.* **2008**, *47*, 2.
[27] Y. Sun, J. A. Rogers, *Adv. Mater.* **2007**, *19*, 1897.
[28] D. Y. Khang, H. Jiang, Y. Huang, J. A. Rogers, *Science* **2006**, *311*, 208.
[29] D.-H. Kim, J.-H. Ahn, W. M. Choi, H.-S. Kim, T.-H. Kim, J. Song, Y. Y. Huang, Z. Liu, C. Lu, J. A. Rogers, *Science* **2008**, *320*, 507.
[30] D.-H. Kim, J. Song, W. M. Choi, H.-S. Kim, R.-H. Kim, Z. Liu, Y. Y. Huange, K.-C. Hwang, Y.-W. Zhang, J. A. Rogers, *Proc. Natl. Acad. Sci. USA* **2008**, *105*, 18675.
[31] Y. Sun, W. M. Choi, H. Jiang, Y. Huang, J. A. Rogers, *Nat. Nanotechnol.* **2006**, *1*, 201.
[32] H. Jiang, Y. Sun, J. A. Rogers, Y. Huang, *Appl. Phys. Lett.* **2007**, *90*, 133119.
[33] W. M. Choi, J. Song, D.-Y. Khang, H. Jiang, Y. Y. Huang, J. A. Rogers, *Nano Lett.* **2007**, *7*, 1655.
[34] J.-H. Ahn, H.-S. Kim, K. J. Lee, Z.-T. Zhu, E. Menard, R. G. Nuzzo, J. A. Rogers, *IEEE Electron Device Lett.* **2006**, *27*, 460.
[35] D.-H. Kim, J.-H. Ahn, H.-S. Kim, K. J. Lee, T.-H. Kim, C.-J. Yu, R. G. Nuzzo, J. A. Rogers, *IEEE Electron Device Lett.* **2008**, *20*, 73.
[36] S. Mack, M. A. Meitl, A. J. Baca, Z.-T. Zhu, J. A. Rogers, *Appl. Phys. Lett.* **2006**, *88*, 213101.
[37] A. J. Baca, M. A. Meitl, H. C. Ko, S. Mack, H.-S. Kim, J. Dong, P. M. Ferreira, J. A. Rogers, *Adv. Funct. Mater.* **2007**, *17*, 3051.
[38] H. C. Ko, A. J. Baca, J. A. Rogers, *Nano Lett.* **2006**, *6*, 2318.
[39] Y. Sun, V. Kumar, I. Adesida, J. A. Rogers, *Adv. Mater.* **2006**, *18*, 2857.
[40] Y. Sun, D.-Y. Khang, F. Hua, K. Hurley, R. G. Nuzzo, J. A. Rogers, *Adv. Funct. Mater.* **2005**, *15*, 30.
[41] Y. Sun, H.-S. Kim, E. Menard, S. Kim, I. Adesida, J. A. Rogers, *Small* **2006**, *2*, 1330.
[42] Y. Sun, E. Menard, J. A. Rogers, H.-S. Kim, S. Kim, G. Chen, I. Adesida, R. Dettmer, R. Cortez, A. Tewksbury, *Appl. Phys. Lett.* **2006**, *88*, 183509.
[43] J.-H. Ahn, H.-S. Kim, K. J. Lee, S. Jeon, S. J. Kang, Y. Sun, R. G. Nuzzo, J. A. Rogers, *Science* **2006**, *314*, 1754.
[44] K. J. Lee, M. A. Meitl, J.-H. Ahn, J. A. Rogers, R. G. Nuzzo, V. Kumar, I. Adesida, *J. Appl. Phys.* **2006**, *100*, 124507.
[45] T.-H. Kim, W. M. Choi, D.-H. Kim, M. A. Meitl, E. Menard, H. Jiang, J. A. Carlisle, J. A. Rogers, *Adv. Mater.* **2008**, *20*, 2171.
[46] D.-Y. Khang, J. Xiao, C. Kocabas, S. MacLaren, T. Banks, H. Jiang, Y. Y. Huang, J. A. Rogers, *Nano Lett.* **2008**, *8*, 124.
[47] M. J. Schultz, X. Zhang, S. Unarunotai, D.-Y. Khang, Q. Cao, C. Wang, C. Lei, S. MacLaren, J. A. N. T. Soares, I. Petrov, J. S. Moore, J. A. Rogers, *Proc. Natl. Acad. Sci. USA* **2008**, *105*, 7353.
[48] Y. Sun, J. A. Rogers, *J. Mater. Chem.* **2007**, *17*, 832.
[49] M. A. Meitl, Z.-T. Zhu, V. Kumar, K. J. Lee, X. Feng, Y. Y. Huang, I. Adesida, R. G. Nuzzo, J. A. Rogers, *Nat. Mater.* **2006**, *5*, 33.
[50] K. Huang, P. Peumans, *Proc. SPIE-Int. Soc. Opt. Eng.* **2006**, *6174*, 617412.
[51] K. Huang, R. Dinyari, G. Lanzara, J. Y. Kim, J. Feng, C. Vancura, F.-K. Chang, P. Peumans, in *Proc. of the IEEE 2007 International Electron Devices Meeting*, IEEE Press, Washington DC, USA **2007**, p. 217.
[52] P. J. Hung, K. Jeong, G. L. Liu, L. P. Lee, *Appl. Phys. Lett.* **2004**, *85*, 6051.
[53] D. S. Gray, J. Tien, C. S. Chen, *Adv. Mater.* **2004**, *16*, 393.
[54] L. Wang, T. Zoumpoulidis, M. Bartek, A. Polyakov, K. M. B. Jansen, L. J. Ernst, in *Proc. of the IEEE 2006 Electronics Packaging Technology Conf.*, IEEE Press, Shanghai, China **2006**, p. 766.
[55] D. Brosteaux, F. Axisa, M. Gonzalez, J. Vanfleteren, *IEEE Electron Device Lett.* **2007**, *28*, 552.
[56] F. Axisa, D. Brosteaux, E. De Leersnyder, F. Bossuyt, M. Gonzalez, M. V. Bulcke, J. Vanfleteren, in *Proc. of the IEEE 6th 2007 Int. Conf. on Polymers and Adhesives in Microelectronics and Photonics*, IEEE Press, Tokyo, Japan **2007**, p. 280.
[57] S. Sosin, T. Zoumpoulidis, M. Bartek, L. Wang, R. Dekker, K. M. B. Jansen, L. J. Ernst, in *Proc. of the IEEE 2008 Electronic Components and Technology Conf.*, IEEE Press, Lake Buena Vista, FL, USA **2008**, p. 1339.
[58] M. Gonzalez, F. Axisa, M. V. Bulcke, D. Brosteaux, B. Vandevelde, J. Vanfleteren, *Microelectron. Reliab.* **2008**, *48*, 825.
[59] B. Huyghe, H. Rogier, J. Vanfleteren, F. Axisa, *IEEE Trans. Adv. Packag.* **2008**, *31*, 802.
[60] S.-I. Park, Y. Xiong, R.-H. Kim, P. Elvikis, M. Meitl, D.-H. Kim, J. Wu, J. Yoon, C.-J. Yu, Z. Liu, Y. Huang, K.-C. Hwang, P. Ferreira, X. Li, K. Choquette, J. A. Rogers, *Science* **2009**, *325*, 977.
[61] K. L. Lin, K. Jain, *IEEE Electron Device Lett.* **2009**, *30*, 14.
[62] N. Bowden, S. Brittain, A. G. Evans, J. W. Hutchinson, G. M. Whitesides, *Nature* **1998**, *393*, 146.
[63] J. Xiao, A. Carlson, Z. J. Liu, Y. Huang, H. Jiang, J. A. Rogers, *Appl. Phys. Lett.* **2008**, *93*, 013109.
[64] S. P. Lacour, J. Jones, S. Wagner, T. Li, Z. Suo, *Proc. IEEE.* **2005**, *93*, 1459.
[65] S. P. Lacour, D. Chan, S. Wagner, T. Li, Z. Suo, *Appl. Phys. Lett.* **2006**, *88*, 204103.
[66] S. P. Lacour, S. Wagner, Z. Huang, Z. Suo, *Appl. Phys. Lett.* **2003**, *82*, 2404.
[67] S. P. Lacour, J. Jones, Z. Suo, S. Wagner, *IEEE Electron Device Lett.* **2004**, *25*, 179.
[68] S. P. Lacour, C. Tsay, S. Wagner, *IEEE Electron Device Lett.* **2004**, *25*, 792.
[69] T. Li, Z. Huang, Z. Suo, S. P. Lacour, S. Wagner, *Appl. Phys. Lett.* **2004**, *85*, 3435.
[70] S. Lacour, S. Wagner, Z. Huang, Z. Suo, *Appl. Phys. Lett.* **2003**, *82*, 2404.
[71] T. Li, Z. Suo, S. P. Lacour, S. Wagner, *J. Mater. Res.* **2005**, *20*, 3274.
[72] Z. Y. Huang, W. Hong, Z. Suo, *J. Mech. Phys. Solids* **2005** *53*, 2101.

© 2010 WILEY-VCH Verlag GmbH & Co. KGaA, Weinheim
WILEY InterScience DISCOVER SOMETHING GREAT

[73] A. C. Siegel, D. A. Bruzewicz, D. B. Weibel, G. M. Whitesides, *Adv. Mater.* **2007**, *19*, 727.
[74] H.-J. Kim, C. Son, B. Ziaie, *Appl. Phys. Lett.* **2008**, *92*, 011904.
[75] H.-J. Kim, T. Maleki, P. Wei, B. Ziaie, *J. Microelectromech. Syst.* **2009**, *18*, 138.
[76] S. Cheng, A. Rydberg, K. Hjort, Z. Wua, *Appl. Phys. Lett.* **2009**, *94*, 144103.
[77] D.-H. Kim, W. M. Choi, J.-H. Ahn, H.-S. Kim, J. Song, Y. Y. Huang, Z. Liu, C. Lu, C. G. Koh, J. A. Rogers, *Appl. Phys. Lett.* **2008**, *93*, 044102.
[78] J. Song, Y. Huang, J. Xiao, S. Wang, K. C. Hwang, H. C. Ko, D.-H. Kim, M. P. Stoykovich, J. A. Rogers, *J. Appl. Phys.* **2009**, *105*, 123516.
[79] H. C. Ko, G. Shin, M. P. Stoykivich, J. W. Lee, D.-H. Kim, S. Wang, J. S. Ha, Y. Huang, K.-C. Hwang, J. A. Rogers, *Small* **2009**, *5*, 2703.
[80] D.-H. Kim, Z. Liu, Y.-S. Kim, J. Wu, J. Song, H.-S. Kim, Y. Huang, K.-C. Hwang, Y. Zhang, J. A. Rogers, *Small*, DOI: 10.1002/smll.200900583.
[81] D.-H. Kim, Y.-S. Kim, J. Wu, Z. Liu, J. Song, H.-S. Kim, Y. Y. Huang, K.-C. Hwang, J. A. Rogers, *Adv. Mater. 21*, 3703.
[82] H. C. Ko, M. P. Stoykovich, J. Song, V. Malyarchuk, W. M. Choi, C.-J. Yu, J. Geddes, III, J. Xiao, S. Wang, Y. Y. Huang, J. A. Rogers, *Nature* **2008**, *454*, 748.
[83] G. Shin, I. Jung, V. Malyarchuk, J. Song, S. Wang, H. C. Ko, Y. Huang, J. S. Ha, J. A. Rogers, unpublished.
[84] I. Jung, G. Shin, V. Malyarchuk, J. S. Ha, J. A. Rogers, unpublished.
[85] S. Wang, J. Xiao, I. Jung, J. Song, H. C. Ko, M. P. Stoykovich, Y. Huang, K.-C. Hwang, J. A. Rogers, unpublished.
[86] L. P. Lee, R. Szema, *Science* **2005**, *310*, 1148.
[87] K.-H. Jeong, J. Kim, L. P. Lee, *Science* **2006**, *312*, 557.
[88] H. C. Jin, J. R. Abelson, M. K. Erhardt, R. G. Nuzzo, *J. Vac. Sci. Technol. B* **2004**, *22*, 2548.
[89] X. Xu, M. Davanco, X. Qi, S. R. Forrest, *Org. Electron.* **2008**, *9*, 1122.
[90] S. M. Miller, S. M. Troian, S. Wagner, *J. Vac. Sci. Technol. B* **2002**, *20*, 2320.
[91] K. E. Paul, M. Prentiss, G. M. Whitesides, *Adv. Funct. Mater.* **2003**, *13*, 259.
[92] H. O. Jacobs, A. R. Tao, A. Schwartz, D. H. Gracias, G. M. Whitesides, *Science* **2002**, *296*, 323.
[93] W. Zheng, P. Buhlmann, H. O. Jacobs, *Proc. Natl. Acad. Sci. USA* **2004**, *101*, 12814.
[94] S. A. Stauth, B. A. Parviz, *Proc. Natl. Acad. Sci. USA* **2006**, *103*, 13922.
[95] P. I. Hsu, R. Bhattacharya, H. Gleskova, M. Huang, Z. Xi, Z. Suo, S. Wagner, J. C. Sturm, *Appl. Phys. Lett.* **2002**, *81*, 1723.
[96] R. Bhattacharya, S. Wagner, Y.-J. Tung, J. R. Esler, M. Hack, *Proc. IEEE* **2005**, *93*, 1273.
[97] S.-B. Rim, P. B. Catrysse, R. Dinyari, K. Huang, P. Peumans, *Opt. Express* **2008**, *16*, 4965.
[98] R. Dinyari, S. B. Rim, K. Huang, P. B. Catrysse, P. Peumans, *Appl. Phys. Lett.* **2008**, *92*, 091114.
[99] J. A. Rogers, Y. Huang, *Proc. Natl. Acad. Sci. USA* **2009**, *106*, 10875.
[100] S. P. Lacour, C. Tsay, S. Wagner, Z. Yu, B. Morrison, III, in *Proc. IEEE Sensors Conf.*, IEEE Press, Irvine, CA, USA **2005**, p. 4.
[101] O. Graudejus, Z. Yu, J. Jones, B. Morrison, III, S. Wagner, *J. Electrochem. Soc.* **2009**, *156*, 85.
[102] J. Viventi, D.-H. Kim, J. D. Moss, Y.-S. Kim, J. A. Blanco, N. Annetta, D. J. Callans, J. Xiao, Y. Huang, J. A. Rogers, B. Litt, unpublished.

© 2010 WILEY-VCH Verlag GmbH & Co. KGaA, Weinheim